To the Graduate Council:

I am submitting herewith a thesis written by Walter Robert Michalchuk entitled "An Investigation of Different Golf Ball Dimple Flow Fields." I have examined the final paper copy of this thesis for form and content and recommend that it be accepted in partial fulfillment of the requirements for the degree of Master of Science, with a major in Aerospace Engineering.

Ahmad D. Vakili, Major Professor

We have read this thesis and recommend its acceptance:

Dr. Uwe Peter Solies

Dr. Charles Limbaugh

Acceptance for the Council:

Vice Chancellor and Dean of Graduate Studies

Thesis
2006
.M53

An Investigation of Different Golf Ball Dimple Flow Fields

A Thesis
Presented for the
Master of Science
Degree
The University of Tennessee, Knoxville

Walter Robert Michalchuk
December 2006

Acknowledgements

I would like to give a special thank you to my advisor, Dr Vakili. His patience and guidance were critical to the success of this project. I also would like to thank the other members of my committee, Dr Limbaugh and Dr Solies for the time they took out of their busy schedules and for the suggestions that they offered. I would also like to acknowledge the hard work and support of Keith Walker, Chris Armstrong, and Jim Goodman at the propulsion lab that were all instrumental in ensuring that his work was a success. A very grateful appreciation goes to Dr Meganathan for his help in the Computational Fluid Dynamics work that was a part of this project. His expertise, hard work and patience were vital in the successful completion of this project.

I would like to thank my friends both here in the USA and at home in Canada for their continued friendship and encouragement along the way. I would also like to thank my mother Nicole and my brother Brian for their support. Finally I would like to thank my wife Georgia who is my best friend and biggest fan. My appreciation for her love and support throughout this endeavor can never be overstated.

Abstract

This experimental study evaluated the potential of various golf ball dimple designs to reduce the drag produced by a golf ball in flight. An experimental setup using four dimple models placed between the leading and trailing edges of a wing section was used. A traditional spherical dimple design was used as the baseline to comparatively study and evaluate the results of the other three different designs. This study was performed on scaled dimple geometries in a water channel at realistic Reynolds numbers. Surface dye flow visualization, pressure measurements and Computational Fluid Dynamics (CFD) were used to evaluate the various designs. Vortex shedding from within a dimple was studied in an attempt to develop a design that improved the vortex strength and increase the energy exchange that takes place between the vortices leaving the dimple and the flow boundary layer beyond.

It was found that a specially designed insert inside the basic dimple provided a means by which flow attachment can take place and vortex strength can be increased. It was also found that the stronger vortices appear to exchange more energy with the flow boundary layer providing it with an improved, fuller profile. It was also found that CFD, if carefully set up, is able to successfully model the flow within a dimple.

Table of Contents

Chapter 1: Introduction	**Page**
1-1: Introduction	1
Chapter 2: Literature Review and Background	
2-1: Literature Review	3
2-2: Background	4
Chapter 3: Experimental Approach	
3-1: Introduction	11
3-2: Dimensionless Modeling	11
3-3: Experimental Model	13
3-4: Flow Visualization	16
3-5: Pressure Measurement	18
3-6: Computational Fluid Dynamics	19
3-7: Dimple Design	21
3-8: Notes Regarding C_D Measurement	24
Chapter 4: Experimental Results and Discussion	
4-1: Flow Visualization Notes	26
4-2: Baseline Dimple	27
4-2-1: Simulation of the Dimple Flow Using CFD-ACE	36
4-2: Flat Bottomed Dimple	38
4-3: Dimple Containing a Small Insert	44
4-4: Large Insert Dimple Design	52
4-4-1: CFD Results	60

Chapter 5: Conclusions and Recommendations

5-1: Conclusions 63

5-2: Recommendations 64

References 65

Appendix A: Drawings 68

Vita 72

List of Figures

Figure	Page
Figure 1: Today's golf balls are manufactures in multiple solid core layers	4
Figure 2: Flow over a smooth sphere	5
Figure 3: Flow within a dimple cavity	6
Figure 4: Flow over a dimple	7
Figure 5: Curves of drag coefficient for smooth and rough spheres and dimpled golf ball; reproduced from Ref. 2.	9
Figure 6: The model used to insert test dimples	14
Figure 7: The dye rake used for flow visualization.	17
Figure 8: Distribution of holes used to measure the pressure inside the cavity and the method used to connect the pressure transducers.	18
Figure 9: Rosemont pressure transducers	20
Figure 10: The baseline dimple	27
Figure 11: Baseline Dimple showing little recirculation	28
Figure 12: A schematic of the separation zone and associated vortex shedding	29
Figure 13: Pressure data obtained inside the baseline cavity	30
Figure 14: Pressure contour plot of the baseline dimple	31
Figure 15: The dispersed wake generated behind the baseline dimple	34
Figure 16: The wake generated by the baseline dimple in relation to the size of the dye stream	35
Figure 17: The geometry used for the 3-D CFD simulations	36
Figure 18: A comparison of the pressure distribution inside the cavity obtained experimentally and through the use of CFD.	37
Figure 19: Fluid recirculation inside the Flat Dimple design	39

Figure 20: Pressure Data obtained for the flat bottomed dimple 40

Figure 21: Pressure Contour plot of Flat Dimple Design 41

Figure22: Improved flow attachment of the flat bottomed dimple 43

Figure 23: The dimple configuration containing a small insert 45

Figure 24: Improved circulation of this design 46

Figure 25: The pressure data collected for the dimple containing the small insert 47

Figure 26: Pressure contour plot of dimple with small insert 48

Figure 27: The increase size and turbulence of the wake created by this design is apparent when compared to those of the previous configurations. 51

Figure 28: Dimple with large cavity insert 53

Figure 29: Recirculation around the large insert 54

Figure 30: Evidence of the forward stagnation point 55

Figure 31: Pressure data obtained for the dimple containing a large insert 56

Figure 32: Pressure contour plot of the dimple containing the large insert 57

Figure 33: The reduced wake and concentrated vortices shed from this design are much improved over the previous designs. 59

Figure 34: The experimental Cp distribution compared to CFD results 60

Figure 35: The grid used for the CFD simulation. 62

Figure A-1: The middle of the support Structure 69

Figure A-2: The main support structure 69

Figure A-3: The baseline Dimple 70

Figure A-4: The flat Bottomed Dimple 70

Figure A-5: The Small Insert Dimple 71

Figure A-6: The Large Insert Dimple 71

Nomenclature

ω	Vorticity
u	Local Velocity
υ	Kinematic Viscosity
V∞	Free Stream Velocity
P∞	Free Steam Pressure
P	Local Pressure
Cp	Coefficient of Pressure
Re	Reynolds Number
ρ	Density
k	Dimple Depth
c	Dimple Diameter
d	Golf Ball Diameter

Chapter 1

Introduction

1-1: Introduction

Over the last several years the golf ball and clubs manufacturing industry has expended considerable resources in efforts to improve the distance balls will travel when hit by players. Much of these efforts have focused on the manufacturing of the clubs used, including the materials used and the design of the clubs and balls. In the past, it has been difficult to improve the aerodynamic efficiency of golf balls as testing was, and remains, very costly and techniques used for modeling lacked the necessary sophistication to provide accurate results. It has only been very recently, with the advent of more sophisticated computer technology resulting in more sophisticated computational fluid dynamics (CFD) models and improvements in experimental data collection that the focus on reducing the drag produced by a ball in flight has been explored in great detail.

The complexity of a golf ball in flight makes it scientifically interesting. Comparing a CFD model of a golf ball to experimental data, obtained through several means including water or wind tunnel testing, provides a meaningful validation of the ability of the model to predict the behavior of other relatively more complex systems. For example, NASA has employed the modeling of a golf ball to predict the behavior of the fuel tanks on the Space Shuttle[1]. Reducing the drag of a golf ball through the alteration of the dimpling has applications in areas such as improving the aerodynamic performance of bridge girders and other similar support structures used in construction areas subject to high wind loading[2]. Other studies have been performed to determine the exact extent to which the dimples of a ball affect its flight and this has led to a greater

understanding of the fundamental principles that are at work. By way of example, Takeyoshi and Tsutahra found that the angle with which a scratch on a ball's surface interacted with the airflow had a significant impact on the behavior of the flow traveling over the scratch.[3]

The present study is intended as an initial step in a series aimed at reducing the aerodynamic drag produced by a golf ball in flight by experimenting with different dimple shapes that have been designed from a fundamental point of view. Further work would need to be carried out to optimize the distribution of the dimples. Study of the distribution pattern is outside the scope of this project. The results published by Ting[4], were used as a basis for further optimization of the dimples to decrease the drag experienced by a ball in flight. The goal of this work is to experiment with various selected shapes and to develop an improved dimple that possibly shows a reduction in the drag produced by the dimples of a golf ball as it is in flight. It is also hoped that these results can be used in other applications where dimple-like structures can be used to reduce the amount of drag produced, and hence reduce the effect of many of the problems associated with aerodynamic drag production in such applications.

This study combines the results of water tunnel flow visualization and pressure measurements to understand the flow around a golf ball dimple. The Computational Fluid Dynamics code CFD-ACE® was used as a tool to evaluate the results obtained for an innovative dimple design that shows improvements in aerodynamic performance.

Chapter 2

Literature Review and Background

2-1 Literature Review

An extensive review of the literature associated with the design of dimples and reduction in golf ball drag was carried out. Details were difficult to obtain because most of the work that has been conducted in the industry is proprietary and not available for review. However, some academic work has been conducted and this was the focus of the literature research. In particular, the work carried out by L.L. Ting [4] and his associates using CFD modeling techniques is referred to in this work. In his work, Ting first demonstrated that the CFD code FLUENT® successfully modeled the flow over a conventional golf ball[5]. Then he proceeded to use the codes to study the effects of altering the depth and diameter of the dimples in order to determine each parameters independent effect on the coefficient of drag (C_D) experienced by the ball as a result of its motion through the air. He did not however validate these results through experimentation, relying on the previous validation of the CFD model chosen as sufficient validation[3].

Several Patents were also studied in order to begin the design process. Several of the patents obtained are currently used by the golf ball manufactures Titleist, Callaway and Wilson and are available in references 15, 16 and 18 respectively.

Interestingly, much more money is spent at present on the internal construction of today's golf balls than the aerodynamics. As in figure 1, which was reproduced from Consumer Report Magazine, nearly all of today's balls are multi-layer solid core balls.[7]

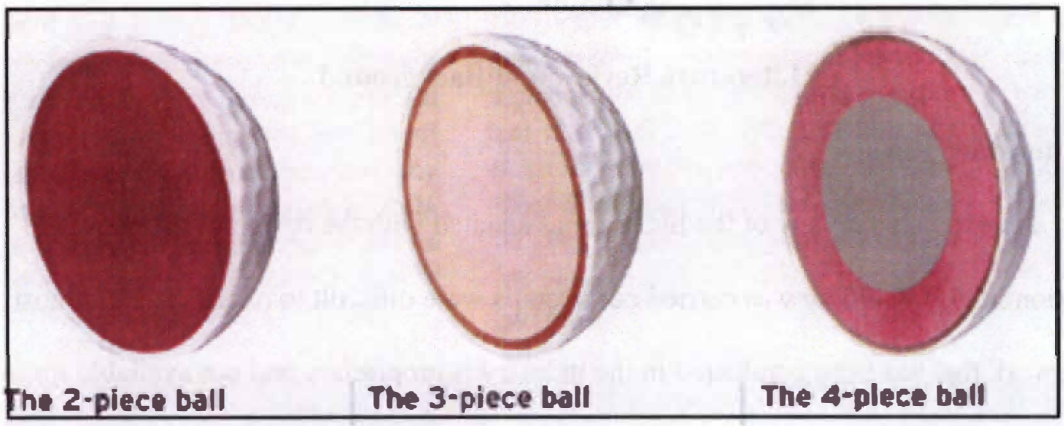


Figure 1: Today's golf balls are manufactures in multiple solid core layers; reproduced from Consumer Report Magazine[7]

Most have two layers, many have three and there are a few that have four layers. The goal of these constructions is to optimize many parameters such as spin rate, launch angle and player feel, to name a few. None of these factors were considered in this work. Again, an optimized dimple will have the same aerodynamic effect on a golf ball regardless of the material used to manufacture it.

Consumer Report also conducted a test on a large number of golf balls. It was determined that within a few yards, most of today's balls travel about the same distance. This implies that both from a manufacturing stand-point and aerodynamically they all perform about the same notwithstanding many of the claims made by the individual manufacturers. [7]

2-2 Background

Lift on a golf ball is generated in the same manner that lift on a circular cylinder occurs as describe in White[6]. It should also be noted that when in flight a golf ball

generates backspin. The backspin is responsible for 20-25% of the lift. However, Ting investigated the effect of backspin in his work. It was concluded that there was no significant effect on drag caused by the backspin.[4] In other words, if a dimple reduces the drag, it will do so whether there is backspin present or not. In light of this, backspin was not considered in this work.

Dimples are an essential component of golf ball design. Optimizing the performance of the dimples has the goal of reducing the total drag coefficient experienced by the ball. Consider a fluid flowing over a smooth spherical object as in figure 2 such that starting at the leading edge stagnation point the flow over the surface of the sphere results in a laminar boundary layer. As the flow travels over the surface of the sphere it encounters an adverse pressure gradient created by the rear stagnation point. The adverse pressure gradient causes the flow to separate readily from the sphere, which in turn creates a large wake behind the sphere resulting in significant drag.[6]

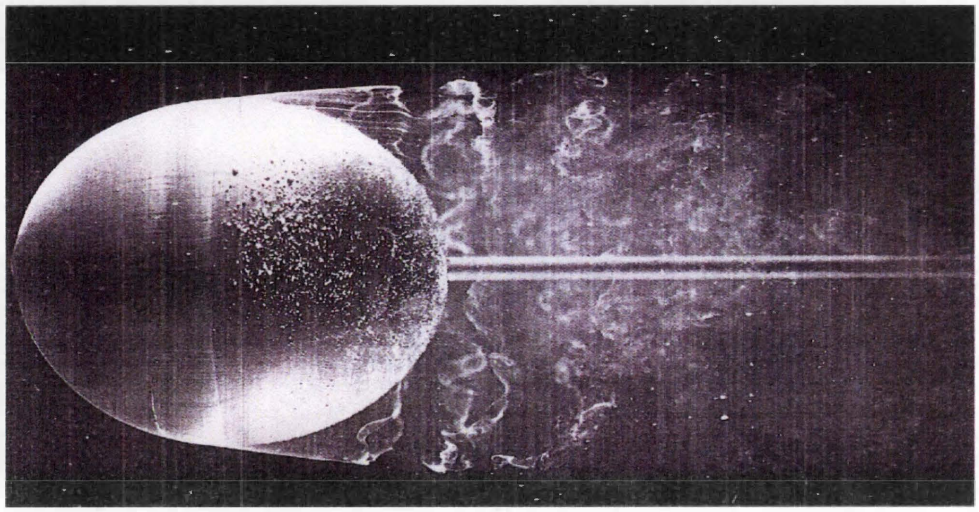


Figure 2: Flow over a smooth sphere; reproduced from reference 25.

Now consider the case of a sphere containing dimples on its surface. As the fluid flows over the surface of the sphere it encounters the leading edge of the dimple as shown in figure 3.

As the fluid enters the dimple a high pressure near stagnation condition exists at the trailing edge. The pressure differential between the trailing edge region and leading edge region causes the fluid to circulate within the dimple and a cavity flow exists. Referring to figure 4, The main flow passes over the cavity, while some enters the cavity and circulates. The creation of turbulence caused by the cavity is the mechanism that allows energy from the main flow to pass on to the boundary layer past the cavity. The turbulence is a result of vortex shedding occurring within the cavity. The flow entering the cavity has a given amount of energy determined by the main flow. Circulation within the cavity takes place, and vorticity is present. Vortices are shed, with a strength determined by the velocity gradients present in the cavity.

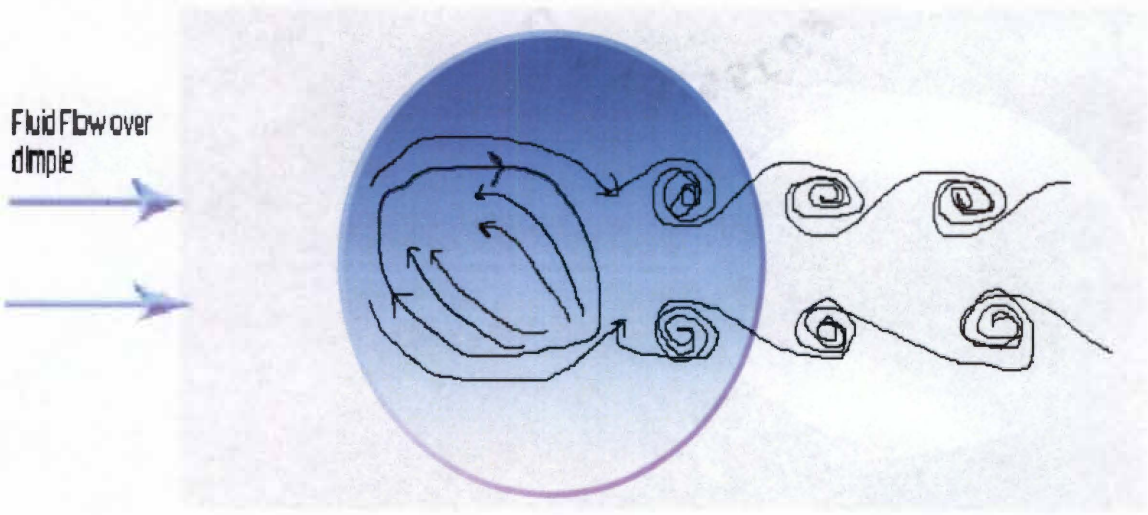


Figure 3: Flow within a dimple cavity.

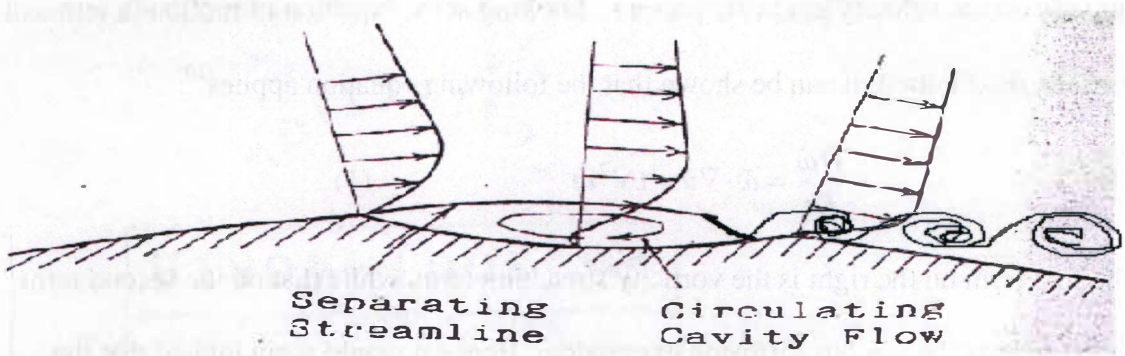


Figure 4: Flow over a dimple; reproduced from reference 2.

Higher kinetic energy within the cavity flow results in higher energy, more concentrated vortices with lesser dispersion upon leaving the cavity. Less dispersion coupled with higher energy vortices result in vortices with a greater ability to draw energy from the main flow as they leave the dimple cavities and mixing of the two flows occurs. The energy drawn out of the main flow is imparted to the boundary layer along the surface of the golf ball through this process. This energized boundary layer is better able to resist the adverse pressure gradient it encounters as it travels along the surface of the ball and encounters the increasing pressure. Because of the turbulence created by the vortex shedding, nearly all references today refer to this type of boundary layer as a turbulent boundary layer.[6] While locally, a turbulent boundary layer creates more drag than a laminar one, globally the flow remaining attached longer reduces the size of the turbulent wake behind the ball, and thus an overall smaller wake and reduction in drag occurs. [19]

While the kinetic energy gradients determines the strength of the vortex shed, the amount of vorticity present in a flow, and in turn the vorticity distribution, depends

greatly on the velocity gradients present. Looking at the equation of motion in terms of vorticity distribution, it can be shown that the following equation applies[10]:

$$\frac{D\vec{\omega}}{Dt} = \vec{\omega} \cdot \nabla \vec{u} + \upsilon \nabla^2 \vec{\omega} \qquad (1)$$

The first term on the right is the vorticity stretching term, while that on the second term on the right is the viscous diffusion expression. Hence it would seem logical that the vorticity of a flow structure can be increase by increasing the velocity gradient present within the flow.

The effect of dimples on a golf ball is very significant on its trajectory in the air. Bearman and Harvey[5] discovered that the drag curve of a golf ball with dimples differs from that of spheres that simply have rough surfaces. Figure 5 shows the results of their comparison. For both the dimpled sphere and the rough sphere the drag coefficient drops at characteristic critical Reynolds numbers. However, as the Reynolds number increases, the drag coefficient of a rough sphere increases while that of the dimpled sphere does not. As a matter of fact the C_D of the dimpled sphere remains constant within the range of Reynolds number beyond the critical Re experienced by a golf ball in flight. From this information Kimura and Tsutahara[2] concluded that there must be another effect caused by the dimple besides facilitation of boundary layer transition.

Dimples are more effective than surface roughness because they are much larger than regular roughness scales, and they are spherical in shape. According to Kimura and Tsutahara[2], the cavity flow that exits within the dimple is not significantly altered over the range of Re of 6.0×10^4 to 3.0×10^5. This explains why the C_D is constant as Re increases while that of the rough sphere increases.

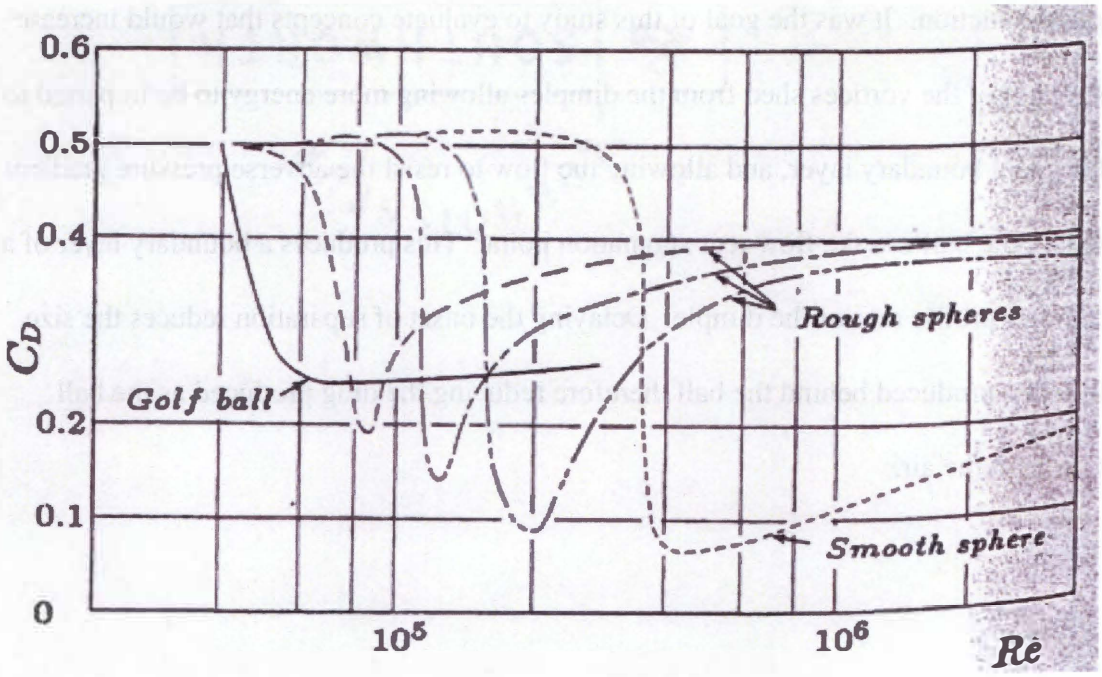


Figure 5: Curves of drag coefficient for smooth and rough spheres and dimpled golf ball; reproduced from Ref. 2.

Furthermore the effect applies to both turbulent and laminar boundary layers. These two facts have an important consequence. When conducting experiments, the results can be assumed valid provided Re is within the range similar to that of the dimpled sphere in figure 5.

Experimentation at lower flow speeds is especially advantageous in the water tunnel where slower speed flows are far more readily handled than higher speed flows, particularly when conducting flow visualization techniques.

While there is some cavity circulation, as discussed, the flow partially travels over the top of the dimple. While the cavity allows energy from the main flow to be imparted to the boundary layer, it also causes a large wake behind the dimple which is responsible for

drag production. It was the goal of this study to evaluate concepts that would increase the strength of the vortices shed from the dimples allowing more energy to be imparted to the turbulent boundary layer, and allowing the flow to resist the adverse pressure gradient caused by the ball's wake flow rear stagnation point. This produces a boundary layer of a much fuller profile rear of the dimple. Delaying the onset of separation reduces the size of the wake produced behind the ball therefore reducing the drag produced as the ball flies through the air.

Chapter 3

Experimental Approach

3-1 Introduction

In attempting to optimize the dimple design, the goal is to delay the onset of flow separation for as long as possible in order to reduce the drag coefficient. In a practical sense this will allow the ball to travel further given the same (flow) conditions.

Using the FLUENT CFD code Ting and his associates found an optimal dimple depth (k) of 0.008587 inches and an optimal dimple diameter (C) of 0.1368 inches. Using the golf ball's diameter (d) to form dimensionless parameters, these values corresponded to a k/d of 0.005 and c/d of 0.08[3]. The dimple described here is the one that was first tested as a baseline for comparison when considering the results of other dimple shapes. In order to vary only one parameter, the diameter and depth of dimples used for testing never changed as it was assumed that these optimal values of depth and diameter would remain so regardless of the shape of dimple employed. Note that in his work Ting discovered that beyond the optimal value quoted here, further increasing the dimple depth had no effect on C_D.

3-2 Dimensionless Modeling

In order to develop a scale model, an estimate of the Reynolds number experienced by a golf ball in flight was required. Using ACCUSPORTS VECTOR LAUNCH MONITOR©, representative ball launch conditions were obtained. The conditions in table 1 were obtained. In its operation, a golf ball travels through a series of highly sensitive lasers. The launch monitor determines the ball's velocity at impact, spin rate and club head speed and determines the distance traveled from the data.[23] The initial

Table 1: Launch Conditions

Initial ball velocity	155 miles/hr
Club Head Speed	115 miles/hr
Backspin Rate	2800 rev/min

ball velocity corresponds to a Reynolds Number (Re) of 2.033×10^5 with the diameter of a regular golf ball dimple (0.137 inches) as the characteristic length. The numbers shown in Table 1 are representative of the author's golf swing, which falls well into the average numbers of amateur golfers. It should be recognized that professionals have higher numbers while other people are below these numbers. However, in each case the numbers will vary by no more than 20%, placing the range of possible Re well within the limits discussed in reference to figure 5[24].

Early on in this work it was recognized that testing a dimple that would be the actual size of that found on a golf ball would be extremely difficult. It was also recognized that a water tunnel would be preferable for flow visualization measurements due to the ease of flow visualization techniques. In order to facilitate testing, scaling of the models would be required using the dimensionless relations k/d and c/d as per Ting's paper. It was decided that a dimple diameter of 5 inches would be appropriate as it would allow for ease of testing. As such scaling of the model for the water tunnel using the Reynolds number and the dimensionless parameters used by Ting was carried out with the resulting scaled parameters listed in table 2. Note that the actual diameter (d) of a golf ball used for play in golf is 1.717 inches.[4]

Table 2: Model Scaling of Test Dimples

	Water
Scaled Ball Diameter (Inches)	58.14
Dimple Diameter (Inches)	5.000
Dimple Depth (Inches)	0.3000
U (ft/s)	5.0

3-3 Experimental Model

Once the full scale dimension of the test dimples was determined, a means of placing it in the water tunnel was required. It was decided that the best way to conduct testing using the water tunnel was to have the dimple installed upside-down. As the hydrostatic pressure is the same at a given depth regardless of the orientation of the dimple, it was not going to affect the results of the tests in any way.[20] It would however make mounting a test item to the water tunnel much easier as the only access to the test section is through the top.

The next area of concern was to ensure that there was steady flow reaching the leading edge of the dimple, without the effects caused by sharp or blunt edges. It was decided that the ideal geometry would be to have geometry similar to the leading edge of a wing at the leading edge of the model, and the trailing edge of a wing at the downstream section of the model.[21] As it turned out, the end product made use of an actual wing section that was available. Figure 6 shows the model that was used. A wing section was cut and the trailing edge and leading edges were kept for use as shown in the water tunnel model in figure 6.

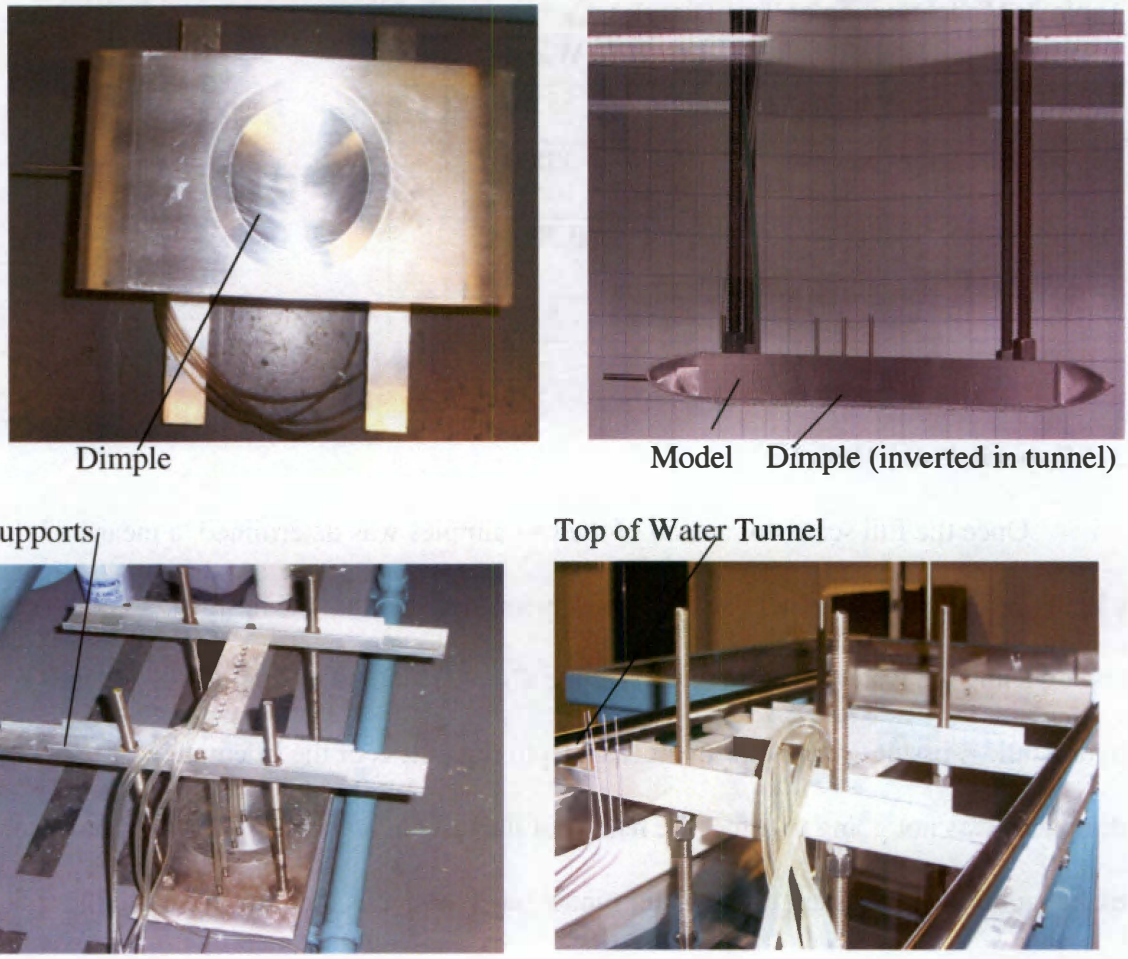


Figure 6: The model used to insert test dimples.

A solid block was then designed, and the center was cut out so that the test dimples could be inserted. The wing sections were then attached to the block to obtain the model shown in figure 6. The engineering drawings for the main block are included in appendix A, figure A-1 and the block and wing section in A-2.

The Drawing in figure A-1 also shows how the dimple was inserted. The hole in the top was stepped, and the dimple inserts themselves were stepped so that they would fit in. The dimple engineering drawings are included in figures A-3 through A-6. The opening in the main model was cut so that the dimple model would fit tightly, but would still be able to rotate. In order to hold the dimple in place once it had been rotated, a plate was attached to the top (towards the top of the tunnel) of the dimple insert through the use of screws which was graduated every ten degrees. With the model installed in the water tunnel, rotating the dimple was simply a matter of loosening the screws, rotating the dimple insert and re-tightening the screws. This allowed testing to occur efficiently. Changing the dimple insert was a matter of taking the screws out completely, removing the insert, and inserting the new one with the plate and the screws.

Each dimple cavity had pressure ports drilled out as per the dimensions in figures A-2 through A-5. These came through the top of the cavity, and the pressure hoses were connected to them at the top. This allowed the user to simply remove them before removing an insert, and simple reattachment once the new dimple insert was installed.

Figure 6 also shows how the model was mounted to the water tunnel. Four large bars were screwed into the top of the model at each of the four corners. The bars were of sufficient size and strength that they were not affected by the loads placed on them by the water flowing through the tunnel, ensuring that the model did not move or vibrate during

testing. A beam was placed connecting each span-wise pair of bars. With the beam in place the model would be held stationary by the top of the water tunnel test section.

3-4 Flow Visualization

As alluded to previously, in order to carry out some quantitative measurements using flow visualization techniques the water tunnel facility at the University of Tennessee Space Institute (UTSI) was employed. The water tunnel was the preferred facility as it far more readily facilitated flow visualization than the low speed wind tunnel facility that was also available. The water tunnel facility at UTSI, capable of a maximum flow speed of three feet per second was used for both flow visualization and pressure measurements.

After some trials, however, it was found at the higher range of velocities a large standing wave is generated which posed two significant problems. The first and most significant is that with the relatively large standing wave generated, static and total pressure measurements would be difficult to obtain. The range of expected pressure measurements is $\pm$1-3 inches of water. A large standing wave, in this case on the order of three inches or more, would introduce significant error to the measurements. The second problem posed by the standing wave is that it introduces a disturbance at depths where the model is located. This makes flow visualization very difficult as the dye stream is affected by the disturbance created by the standing wave. Flow speed of approximately 1 foot per second was settled upon after some trial and error. This places the Re at 6.7×10^4 still within the range of constant C_D found by Kimura and Tsutahara[2]. Further supporting this decision was the work carried out by McDaniels in a similar facility at UTSI. In his

work, McDaniels found that in modeling a higher Re flow with a lower Re flow, the qualitative details remain in tact. [14]

The dye selected to carry out the flow visualization observations was formulated to be neutral density with respect to the water in terms of specific gravity. This made the dye neutrally buoyant allowing for proper boundary layer observations to be undertaken. Before measurements were made, the density of the dye was tested to ensure that it was in fact the same as the water. As a matter of detail, the color of the dye used was changed so that it would show up better in pictures. This did not however change the composition of the dye nor its buoyancy.

In order to inject the dye into the flow, dye injection probes, the apparatus shown in figure 7 was used. The dye is forced under pressure into steel tubing. The tube ends in a four pronged rake that injects the dye into the flow in a very tight stream. In some cases the dye is injected upstream from the dimple model to observe the flow as it encounters the dimple. In other cases the flow is injected directly inside the dimple itself with the water not flowing in order to entrain it in the cavity in an attempt to observe what happens when the flow starts. Another advantage of running the water tunnel at low speed is that the disturbance caused by having the rake upstream is negligible and thus not considered a factor.

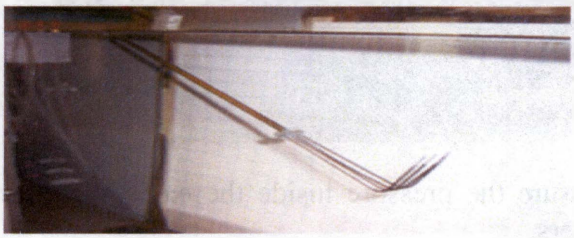


Figure 7: The dye rake used for flow visualization.

3-5 Pressure Measurement

In order to obtain an estimate of the pressure variations within the dimple, it was decided to drill three small pressure ports into the cavity as shown in figure 8. Connected through tubes coming out of the top of the model to pressure transducers, the pressure was measured at each of the three locations. By rotating the dimple in ten degree increments a distribution of the pressure within the complete cavity was obtained.

Finding suitable pressure transducers proved to be difficult.

Initially pressure transducers where installed such that water entered partially in the tube and would cause the air pressure at the transducer to increase. This however produced unacceptable unstable results. As mentioned, the expected range of pressure measurements was on the order of $\pm$ 1-3 inches of water.

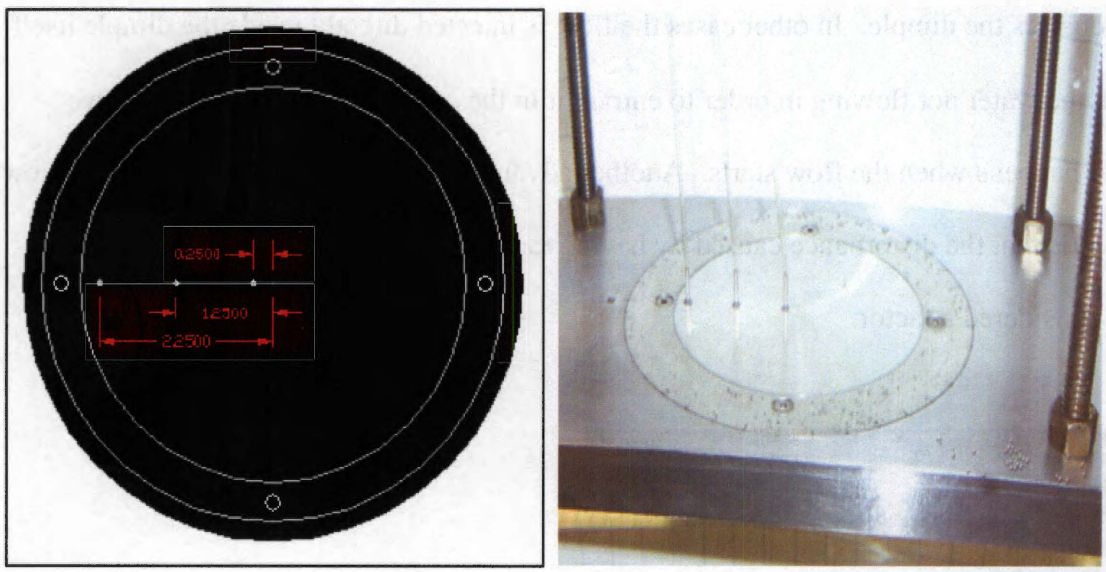


Figure 8: Distribution of holes used to measure the pressure inside the cavity and the method used to connect the pressure transducers.

The problem with this set up was that the tubes that were used were very small and the water would not completely drain from them. The water that remained in the tube was enough to cause a 40-50% error as compared to the value measured. This was not acceptable.

The setup in figure 9 was tried and found to be successful. In this set up Rosemont® transducers are connected to the tubing. These have the advantage of having the capability of coming into contact with water thus alleviating the problem caused by having an air water interface.

Initially pressure transducers whereby the water in the tube would cause the air pressure at the transducer obtained the coefficient of pressure and distribution could be obtained. This data could then be compared to the results of the computation fluid dynamics code discussed later. The Rosemount transducers were spanned so that they could measure the pressure from negative $\pm$ 3 inches of water. The transducers are also capable of measuring pressure to 0.001 inches of water. It was estimated that the error in the readings provided by the transducers was $\pm$ 0.5% of maximum range. The automated system collected 10 data points per second, each an average of 1000 readings. The Root mean squared method was used to obtain the error estimates. [12]

3-6 Computational Fluid Dynamics

With the advent of faster and more powerful computers, computational fluid dynamics is now at the forefront of fluid dynamics study. Simple flows such as the classic problem of flow over a cylinder to much more complex ones describing the flow over the entire surface of an aircraft can be modeled with CFD.

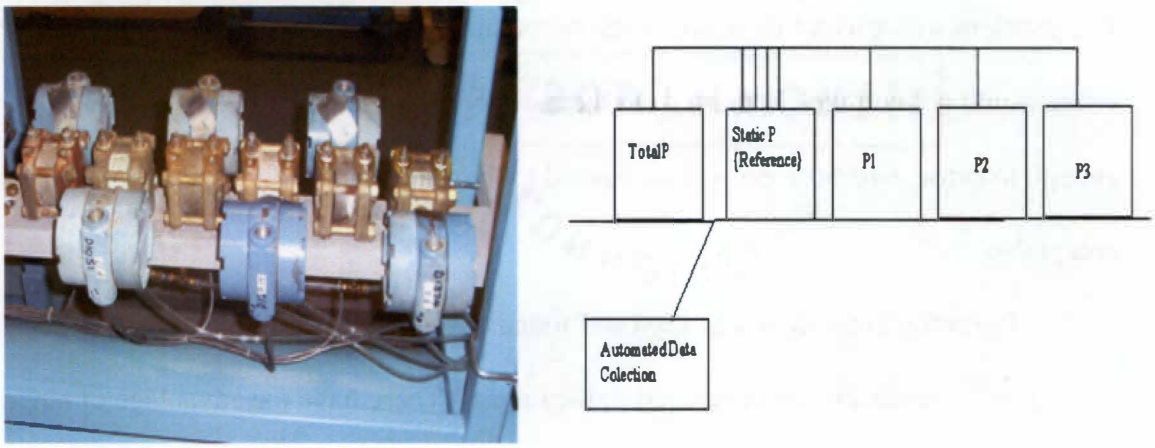


Figure 9: Rosemont pressure transducers.

CFD has the advantage of allowing designers and researchers to study flow and determine desired parameters with out running very costly, or in some cases nearly impossible, experimental tests in order to obtain the desired information. That being said, validation of the results obtained from a code using a basic well understood test item is always necessary before the information provided by the CFD code can be used with any degree of confidence.

In this work CFD was used in order to determine pressure distribution as well as information regarding the vortex behavior present in the final design. Before doing so however, the baseline dimple described below was modeled using a CFD code and compared to the results obtained experimentally in order to validate using the code accurately.

The meshing program that was used is CFD-GEOM®, while the CFD code used was CFD-ACE®. The first step in the validation process was to obtain some experimental results for the baseline dimple and develop a 2-D CFD code that accurately models that observed by experiment. The advantage to doing this is that the computer

processing required to run a 2-D code is far less than that of a 3-D code, and therefore trouble shooting and variation of the numerous parameters associated with the code can be carried out far more quickly.

Once an acceptable 2-D code was developed and results found to satisfactorily model what was observed by experimentation, a 3-D code was used to complete the validation process. The 3-D code is processor intensive and requires a lengthy amount of time to run. However, once the various parameters have been adjusted properly, the resulting 3-D model provides an excellent tool for studying the expected pressure velocity and vorticity distributions. Of course, the results obtained using the 3-D code was once again checked to ensure that they accurately reflected the observed phenomena.

Once the baseline code provided satisfactory results, it was used to model the flow parameters of the final design, the large mountain dimple described below. Those results that could be obtained experimentally were compared to ensure the model accuracy in order to determine is viability as a means of studying future designs.

3-7 Dimple Design

As mentioned in an earlier section, golf ball dimples are designed such that there exists an internal cavity flow. Many studies have been conduced that changed the depth, diameter and the distribution of dimples on a golf ball, including the work done by Ting [4] and his associates. In addition, the Callaway and the Wilson companies have developed dimples of hexagonal and flat-bottomed shapes respectively as outlined by the patents in references 15 and 16. Despite this effort, independent testing such as those carried out by Consumer Reports magazine in reference 7 discussed previously have shown that aerodynamically, all of these balls perform nearly equally.

In order to improve the aerodynamic performance of a dimple, one may conclude that a fundamental change in the behavior of the flow inside and within the vicinity of the dimple is required.

As discussed in reference 2, there is a portion of the flow that passes over the dimple while a small portion of the flow is brought into the dimple where the action of its circulating within the cavity helps to re-energize the flow passing over the cavity. The increased energy allows the flow to remain attached to the surface of the golf ball more readily once it passes the dimple as it is better able to resist the adverse pressure gradient created by the balls aft stagnation point.[6] The global effect is that the flow over the sphere remains attached longer and the size of the wake behind the ball is reduced, thus reducing the drag.[6] In considering different design possibilities, the goal is to impart as much energy to the boundary layer of the main flow after passing over the cavity as possible. Even a modest increase in the energy imparted to the flow on the order of 10-20% can significantly reduce the aerodynamic drag produced by a dimple as this represents a large increase in the flow's ability to overcome adverse pressure gradients.[6]

At the leading edge of a dimple the flow coming from upstream separates from the surface of the ball. The majority flow continues over the dimple while a very small portion of it circulates inside the cavity. In order to increase the amount of energy imparted to the main flow boundary layer, it would be desirable to increase the strength of the vortices shed from the cavity. To accomplish this, the local velocities and velocity gradients inside the cavity must be increased. As discussed before, this has the effect of reducing the wake both aft of the dimple and globally.[2]

In order to have the flow reattach to the surface of the sphere, it was hypothesized[20] that a "insert" centered over the center of the dimple cavity would provide a surface for the flow to reattach to. With the larger surface of the insert providing a means of attaching the flow, it was supposed that a greater portion of the total flow passing over the cavity will be brought in and move around the insert. Attaching to the surface of a insert also increases the velocity of the flow circulating within the cavity and increasing the kinetic energy available. It was hypothesized that the mixing of the two flows would increase the energy of the flow beyond the dimple thus allowing the flow to remain attached to the surface of the golf ball, and reducing the drag.[2]

While ideally the insert could extend higher than the leading edge surface of the diameter of the ball, practically this is not possible. During the contact between the golf club and the ball, a large amount of deformation takes place due to the significant amount of force that is involved. Because of this, having the insert extend outside of the cavity would mean that within a small number of strikes, the insert would lose its effectiveness as it would be crushed or damaged in some fashion.

In order to test the effects of a insert inside the cavity, four dimples were built. The first one was a standard scaled dimple shape with the optimal depth and diameter that was determined by Ting.[4] In order to reduce the number of variables involved, this was also the depth and diameter of each of the test dimples studied. The second dimple studied was based on the patent in reference 18 produced by Wilson. In this design, the bottom of the cavity is flat similar to a frying pan. In the patent, the designer of the dimple states that it shows improved performance over a standard shaped dimple in that it reduced the overall drag produced.[18] The third dimple was built having a mountain insert

in the cavity that extends to 0.05" below the top of the dimple cavity, with a top diameter of 0.25" and the sides sloping 45^0. The final dimple was similar to the third; however the top diameter of the mountain was increased to one inch. It was hoped that these configurations could be compared to both the baseline dimple and the flat bottomed dimple and would show improvement in terms of the size of the wake generated as the flow leaves the cavity.

Finding suitable pressure transducers proved to be difficult. Initially pressure transducers whereby the water in the tube would cause the air pressure at the transducer to increase were tried. This however produced unacceptable results. As mentioned, the expected range of pressure measurements was on the order of $\pm$ 1-3 inches of water.

3-8 Notes Regarding C_D Measurement

Unfortunately, it is impossible to directly measure the coefficient of drag with the resources available at UTSI. However, using flow visualization it is possible to obtain a qualitative assessment of whether or not the aerodynamic drag wake behind the dimple is reduced or not. Observations such as the size of the wake, the amount of flow brought into the cavity and the degree to which the flow remains attached to the surface after the dimple can be compared amongst the various models. While these types of observations are valuable, highly accurate measurements would be preferable but are not possible due to resource limitations. The information obtained is still important as it may help determine whether future, more costly, testing is warranted.

Measuring the pressure distribution within the cavity is in contrast very accurate, and provides a direct quantitative comparison of the performance of each cavity through the use of non-dimensional coefficients, namely the pressure coefficient.

The CFD code also provides a very accurate comparison of the performance of each respective cavity in addition to providing an excellent means of validating the results obtained experimentally.

Chapter 4

Experimental Results and Discussion

4-1 Flow Visualization Notes

The dye used to carry out the flow visualization experiments is a mixture of ethanol, short-chain polymer, and water. The ingredients are mixed in proportions necessary to ensure the specific gravity is as close to water as possible. Prior to running the experiments, it was important to ensure that the dye used was neutrally buoyant with respect to the water in the tank. In order to test the dye, the water tunnel was turned off and sufficient time was allowed for the water to settle. A drop of dye was placed in the tunnel. If it sank, its specific gravity was high and ethanol was added to reduce the specific gravity. If it rose, polymer was added. This adjusting process continued until the drop would remain still in the water, indicative of it having the appropriate specific gravity.

Because of some problems associated with running the tunnel at higher speeds, namely the presence of a standing wave at higher speeds, and that slower water speeds facilitate visualization, the tunnel was adjusted such that the flow velocity was approximately one foot per second. Note that this places Re at approximately 6.7×10^4, within the range studied by Kimura and Tsutahara[2] as discussed earlier. The pressure measurements were conducted at approximately 2.0 feet per second. This was necessary in order to have pressure values within the range the transducers were capable of measuring with accuracy. As per the previous discussion, the visualization observations made would still be valid at this speed.

4-2 Baseline Dimple

The first dimple shape studied was the one shown in figure 10. The spherical shape of the cavity itself is based on the current design patent in reference 15 which is currently in use by the Titleist Company as the standard dimple shape in its golf balls. The design was altered slightly using the results that Ting and his associates obtained. The optimal depth and diameter quoted in Ting's work was selected as it represented the configuration that produced the least amount of drag. A more meaningful comparison of the performance of the designs obtained in this work could be achieved in this manner.

In order to study the recirculation inside the dimple cavity the dye probes were placed inside the cavity such that they were in contact with the surface. With the flow running dye was injected into the dimple and the streaklines were digitally recorded. Figure 11 shows a still image taken from one of the videos. There is a small region of recirculation occurring in the dimple. Within a short distance from the dimple beginning, there are vortices shed and the flow is separated and leaves the cavity.

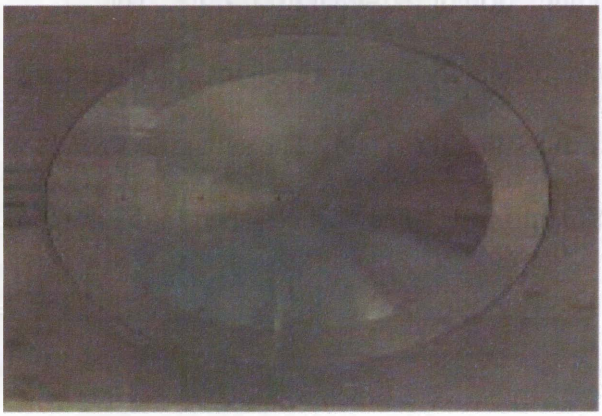


Figure 10: The baseline dimple.

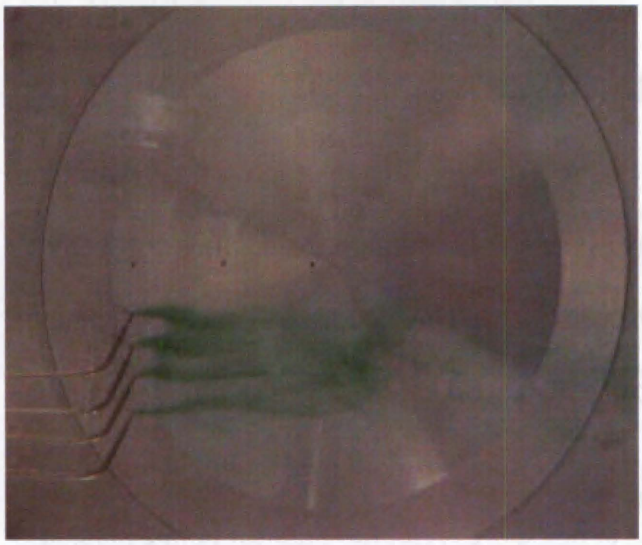


Figure 11: Baseline Dimple showing little recirculation.

While difficult to see in figure 11, it is obvious from the video analysis that there is a very small portion of the dye that gets drawn into the cavity and circulated within.

Observations of the cavity by entraining fluid into the dimple led to the discovery that there is a large separation zone created at the front of the dimple as the fluid meets its leading edge. The separation zone is important because it is in this zone that vortices are formed and shed in the fluid. Figure 12 is a depiction of the separation zone. The separation zone starts at the leading edge were the cavity curvature begins and extends approximately 40% into the cavity before vortices begin to shed. The separation zone follows the curvature of the leading edge of the dimple. The vortices shed in this region disperse rapidly.

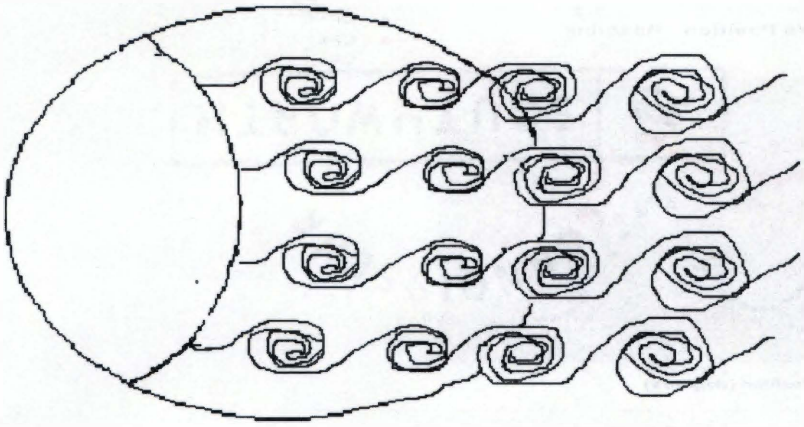


Figure 12: A schematic of the separation zone and associated vortex shedding

At first it was not known why so little of the flow was being drawn into the cavity. However, study of the pressure distribution within the dimple provided the answer. Figure 13 is a plot of the data that was obtained by measuring the pressure within the cavity and calculating the coefficient of pressure (Cp). As a matter of reference CP1 is the data that was collected from the pressure port 2.25 inches from the center of the cavity, while CP2 and CP3 were measured moving inward toward the center as per figure 8. The data was collected in 10 degree intervals along the 360 degree circular cavity. It can be seen from the plot that CP3 remains nearly constant except for the region between 130 degrees and 280 degrees where there is a sharp increase in the value of CP3. Cp is defines as follows:

$$Cp = \frac{P - P_{\infty}}{\frac{1}{2}\rho V_{\infty}^{2}} \qquad (2)$$

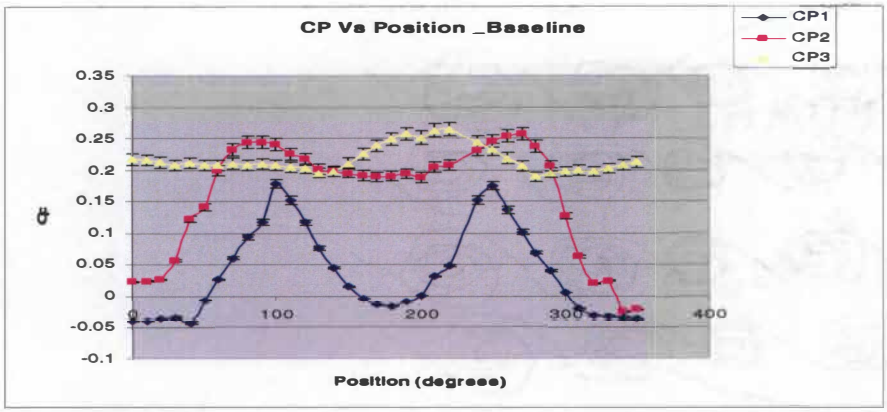


Figure 13: Pressure data obtained inside the baseline cavity.

The increase is on the order of 20%, which reflects a drop in the velocity of the fluid in the cavity in this region. This also marks a region where flow separation has increased. Note that this region is fairly large. CP1 varies from nearly zero, with peaks occurring at approximately 100 and 250 degrees with a valley near 180 degrees. The peaks are areas were separation is centered, hence the higher value in CP while the valley represents a region where flow circulation and vortex shedding is occurring. CP 2 shows a similar trend with higher overall values of the coefficient of pressure as CP2 is more inside the separation bubble. There is an asymmetric behavior though to be due to flow alignment relative to the model axis may not have been exact.

The contour plot in figure 14 was obtained by taking the pressure measurement data from figure 13 and interpolating it to cover the entire surface of the cavity. The interpolation does introduce some uncertainty into the plot. However, comparison of the visual observations made from figure 11, and the CFD results, discussed later show good agreement. The black dots represent actual data points.

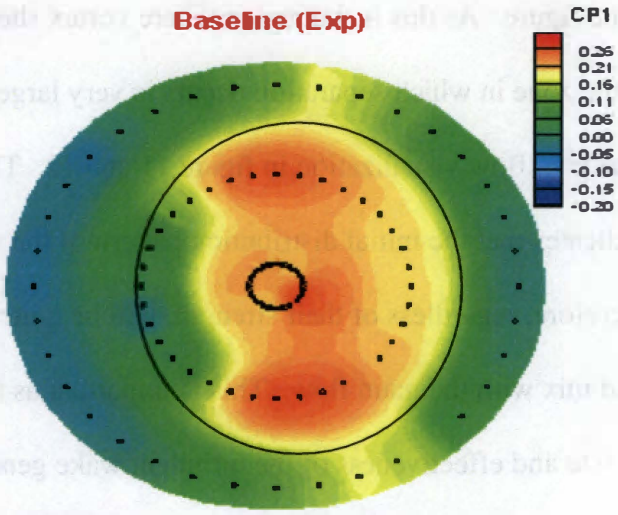


Figure 14: Pressure contour plot of the baseline dimple.

Examining the pressure contour plot in figure 14, the area in green represents the area where the flow is recirculating in the cavity. Note that in this region, the speed of circulation is slow as indicated by the relatively high pressure. The overall low velocities present throughout the cavity explain the difficulty experienced during flow visualization where it was difficult to get dye to circulate within the cavity. There simply was not sufficient speed present to bring dye into the cavity.

The yellow and red region circled corresponds to the area where CP3 shows an increase in figure 13. This area is of particular importance as this is the region where vortex shedding is occurring and there are several important results that can be obtained through study of this area. Note that the yellow indicates that flow in this region is moving at a very slow velocity while the red region indicates nearly separated flow.

The first observation is regards the size of the region in the X-Y plane. The circles area is very large in relation to the overall area of the cavity, whose boundaries

match those in the figure. As this is the region where vortex shedding is occurring, this region shows that the zone in which separation occurs is very large, which agrees with the observations made in flow visualization in figure 11 and 12. This large region of separation zone indicates that the initial distribution pattern of the vortices when shed is quite large, and therefore, regardless of their strength, will be quite dispersed as they leave the cavity and mix with the main flow. This is important as it is one of the factors that determine the size and effectiveness of the turbulent wake generated by the dimple.

Figure 14 contains information regarding the total vorticity of the flow in the cavity. It was observed through flow visualization that the period between successive vortices being shed is relatively long as compared to the other designs tested. Figure 13 explains in part why this is the case. The difference in velocities within the circled region from one point to the next are not significantly high resulting in low velocity gradients. Looking once again at equation (1):

$$\frac{D\vec{\omega}}{Dt} = \vec{\omega} \cdot \nabla \vec{u} + \upsilon \nabla^2 \vec{\omega}$$

From this equation we can see that the rate of change of vorticity, described by the first term on the right is highly dependent on the velocity gradients present. The gradients in the X-Y plane are minimal as can be seen in figure 13. Also of interest is the velocity gradient in the Z direction, defined for this work as the direction normal to the plane of the cavity. In this direction the distance between the bottom of the cavity, approximately where separation is occurring, and the main flow is nearly equal to the depth of the cavity, in this case 0.30 inches. While the difference between the main flow velocity and the re-circulation velocity may be high, the distance between them is small, and thus the

gradient in this direction is very small in magnitude. Because of the low gradients present, the vorticity of the flow within the cavity is low resulting in vortices being shed with relatively large periods between consecutive occurrences.

The low speed cavity flow means there is minimal kinetic energy. This has two important consequences. In terms of the vortex shedding, the low energy of the circulating flow is important as it relates to the strength of the vortices when shed. It was observed during flow visualization that the individual vortices disperse very rapidly after they have been shed, this is as a result of the low energy concentration they contain when produced. Combining the fact that they are shed in a largely scattered pattern the rapid dispersion of the vortices is a large factor in determining the size of the wake produced by a dimple as the flow interacts with it.

Because of their rapid dispersion, and their low strength, the vortices shed by the baseline dimple have minimal capacity to draw energy from the main flow. Consequently, there is minimal energy imparted to the turbulent boundary layer of the main flow traveling along the surface of the golf ball by the mechanism described in section 1. The low energy transfer results in a minimal improvement in the main flows ability to overcome the adverse pressure gradient it encounters. It is still an improvement as compared to that of flow over a smooth sphere, however, the result is a minimal reduction in the size of the wake produced by a golf ball in flight, and therefore there is still significant aerodynamic drag produced by the baseline dimple.

As mentioned previously, the vortices that are shed disperse rapidly. Figure 15 shows a side view of the flow leaving the dimple cavity. In this trial dye was injected into the cavity in the approximate area of the separation zone. In the photograph it is



Figure 15: The dispersed wake generated behind the baseline dimple.

clearly visible that by the time the flow has left the cavity the vortices are highly dispersed. In addition, they are traveling separated by quite some distance from the surface of the model. This is indicative of the low energy with which the flow left the cavity. It is unable to remain attached to the surface of the model, which is representative of the surface of a golf ball, and so separation occurs. Because it is losing energy due to the viscosity of the water in the tunnel, which was included in the scaling process of the water, the flow at this point contains very little energy and the dispersion and separation from the surface of the model creates a large wake. It is the presence of this large wake that is responsible for most of the drag experienced by a golf ball in flight. This experiment was run twice to confirm the results as the other configurations showed very significant improvements in this area.

Figure 16 is a top view of the wake that is generated as a result of the flow interacting with the cavity. Here the dye was introduced into the flow upstream of the leading edge. The lines drawn are intended to bring to attention the size of the wake generated in relation to the size of the dye stream fed into the flow. The ratio of the wake size to the dye stream size was found to be approximately 1.5. This is qualitatively significant as it is apparent that the wake is substantially larger than the initial stream fed to the cavity. While this wake is not as large and not as dispersed as it would be behind a smooth sphere, it is still a significant source of drag production.

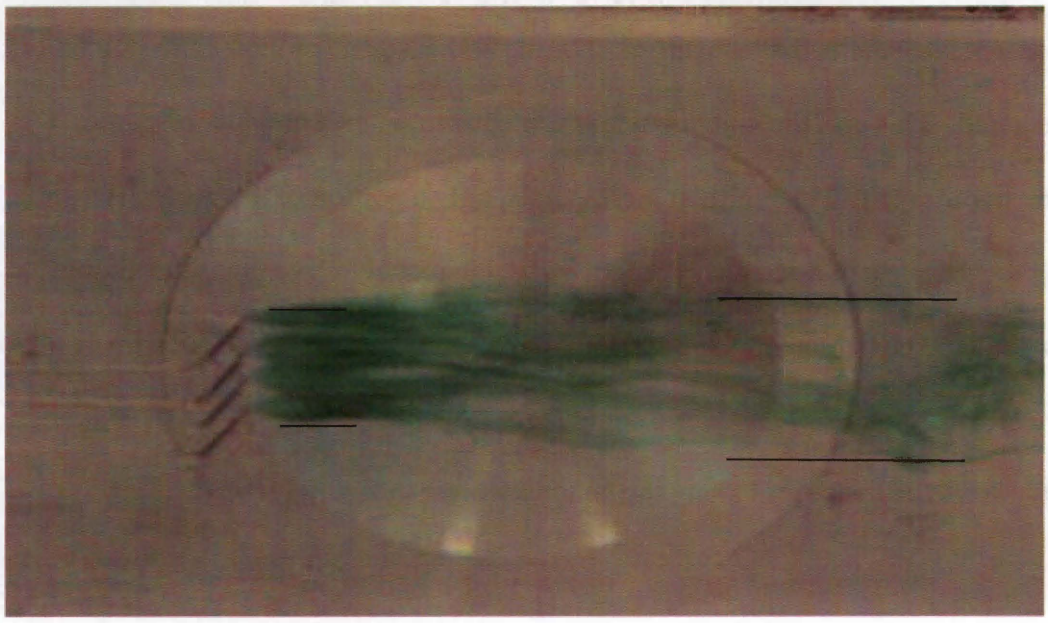


Figure 16: The wake generated by the baseline dimple in relation to the size of the dye stream.

4-2-1 Simulation of the Dimple Flow Using CFD-ACE

CFD-Ace is a Navier-Stokes solver. Both unsteady and steady flow models were studied. In the 2-D cases that were run unsteady flow was simulated. While this would also have been appropriate, this was not possible due to the time required to run with the computing resources that were available.

In the steady cases, the K-ϵ turbulence model was used, while for the unsteady cases, the Large Eddie Simulation (LES) turbulence model was used. In both cases the turbulence intensity was set to 1%. This parameter was studied through several trials and 1% was the value found to provide results that best agreed with experimental data.

For the 2-D simulations, approximately 200,000 mesh points were required to provide acceptable results that converged. For the 3-D case one million mesh points were generated. This was the maximum allowable based on the computer resources available. In order to use one million mesh points, only a portion of the geometry including the dimple and a section of length and height equal to five times the dimple diameter could be constructed. It was assumed this would remove any possibility solid boundary effects. Figure 17 shows the complete 3-D geometry as well as a slice through the cavity. Note the dense grid along the boundary layer in figure 17(b).

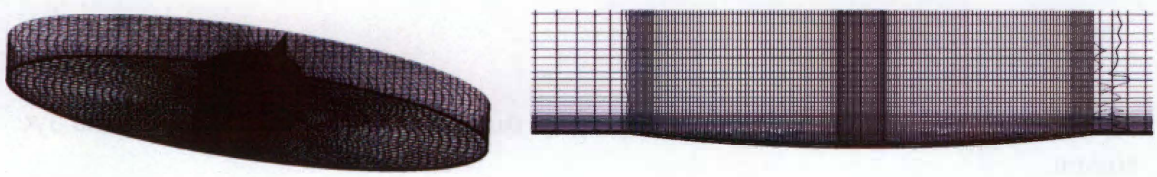


Figure 17: The geometry used for the 3-D CFD simulations.

Figure 18 shows the pressure distribution inside the cavity obtained from running a 3-D CFD code using CFD-ACE next to the same plot shown in figure 14. As figure 18 shows, the results of the CFD analysis generally agrees very well with the experimental results. The blue region on the leading and trailing edges of the plot obtained through CFD are a result of a small region of flow separation due to the geometrical discontinuity that exits only in the CFD model, and do not show up on the experimental plot. The size overall size of the region in red, where vortex shedding occurs, is nearly the same size in both plots. The CFD code predicts slightly slower velocities around the outer edges of the dimple as the yellow region of the plot is somewhat larger than that shown in the experimental plot. Note that the velocity difference in the area is minimal. It is assumed that some of this difference is a result of the interpolation process that was used to plot the experimental results.

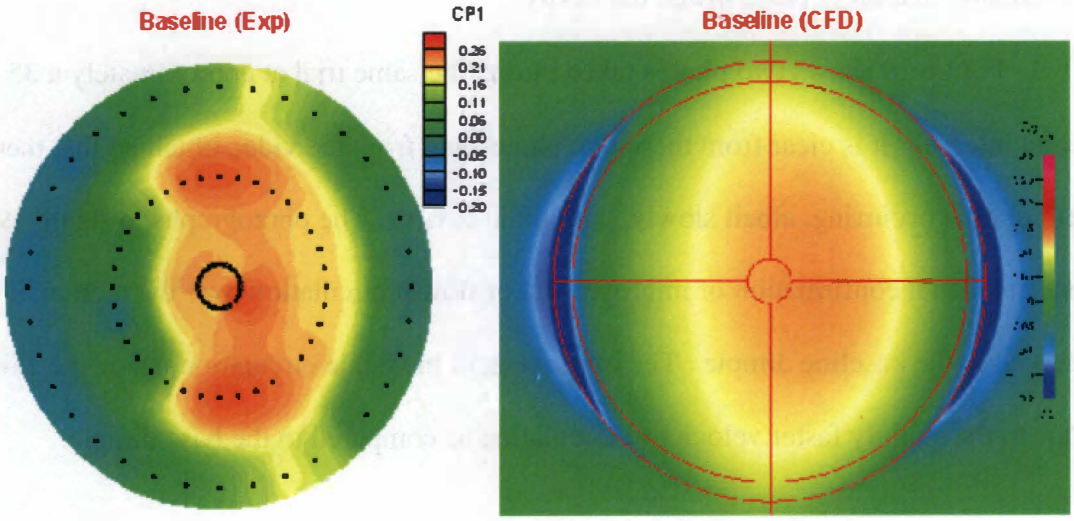


Figure 18: A comparison of the pressure distribution inside the cavity obtained experimentally and through the use of CFD.

However, it can be readily seen that the results shown here compare very well, indicating that both the interpolation process and the CFD model can be used to predict the flow. Consequently, the experimental results obtained can be used with confidence. In addition the CFD code can be used to obtain results that can not be obtained experimentally with confidence that they will be sufficiently accurate to provide meaningful information. It should be noted that the experiments conducted were an unsteady process while the 3-D code was a steady simulation. If the code could have been run with an unsteady model, the result would have been similar to that obtained with some minor differences.

4-2 The Flat Bottom Dimple

The next dimple shape that was studied was the flat bottomed dimple, as patented by Wilson in reference 19. As expected, there is a separation zone very similar to the one for the baseline dimple. There is however a slight improvement in the amount of recirculation that takes place inside the cavity.

Figure 19 shows two photos taken during the same trial at approximately a 35 second interval. It is clear from these two photos and from the video obtained that there is circulation occurring, albeit slowly, within the cavity. The photographs in figure 19 represent visual confirmation of improvement of flow recirculation over the recirculation observed in the baseline dimple. The improvement in visible circulation inside the cavity is due to the slightly faster velocity of circulation as compared to the base dimple.

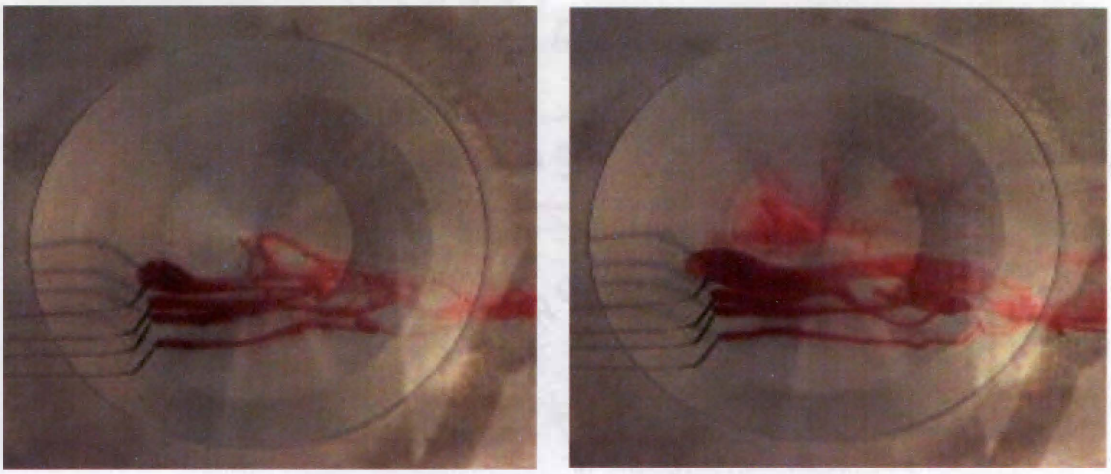


Figure 19: Fluid recirculation inside the Flat Dimple design.

The plot in figure 20 is the pressure coefficient data that was measured for this configuration. It shows much of the same trends as the baseline dimple plot of figure 13 however, there are some notable differences. The most striking is the difference in the behavior of CP3 near the center of the cavity. Whereas the baseline dimple showed a marked peak, the plot in figure 20 shows a nearly constant value throughout.

In the region were the peak in the baseline CP3 occurs this configuration represents a decrease in CP3 of approximately 20%, with a similar improvement in the velocity of the circulation in this region, there is a definite improvement in this region in terms of the circulation for this configuration. CP1 displays little change from that of the plot for the baseline. CP2 also shows a similar trend as that obtained for the baseline, however there is a small increase in CP2 of about 15% around the 180 degree region in this configuration.

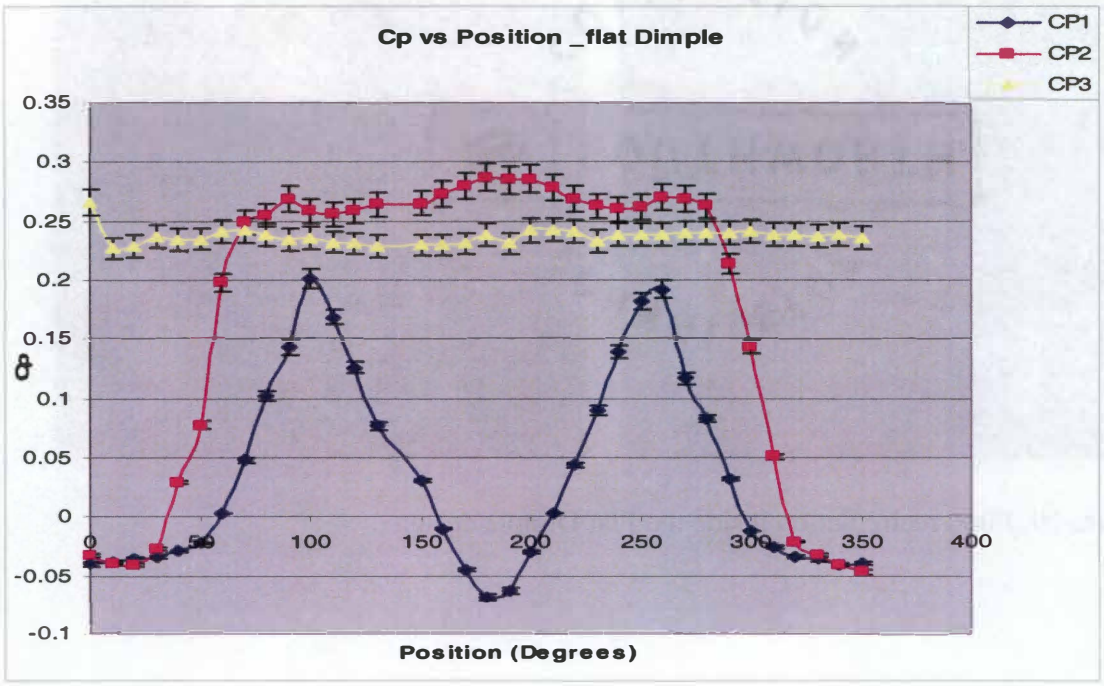


Figure 20: Pressure Data obtained for the flat bottomed dimple.

This is the rear region of the dimple cavity, and it is thought that this is due to more concentrated separation taking place here.

The faster circulation velocity also allows more of the flow to be brought into the dimple cavity from the main flow passing over the top as it results in a lower pressure in the cavity, and therefore a higher pressure gradient between the cavity and the main flow.

Figure 21 is a pressure coefficient contour plot obtained from the pressure data measured within the cavity. Again, the pressure data collected was used to interpolate the plot over the entire surface of the dimple. It is, as was the case with the baseline dimple, subject to some uncertainty, however, as discussed the results can be used with reasonable confidence as they do reflect trends viewed visually.

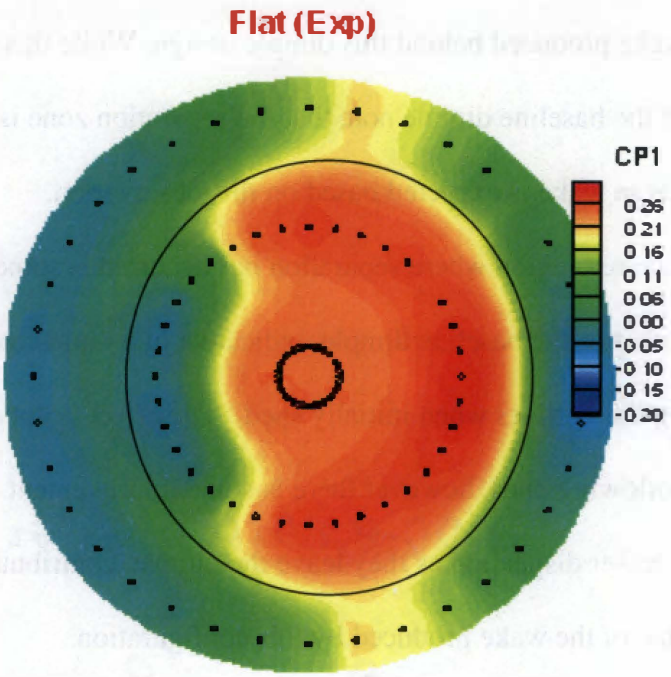


Figure 21: Pressure Contour plot of Flat Dimple Design.

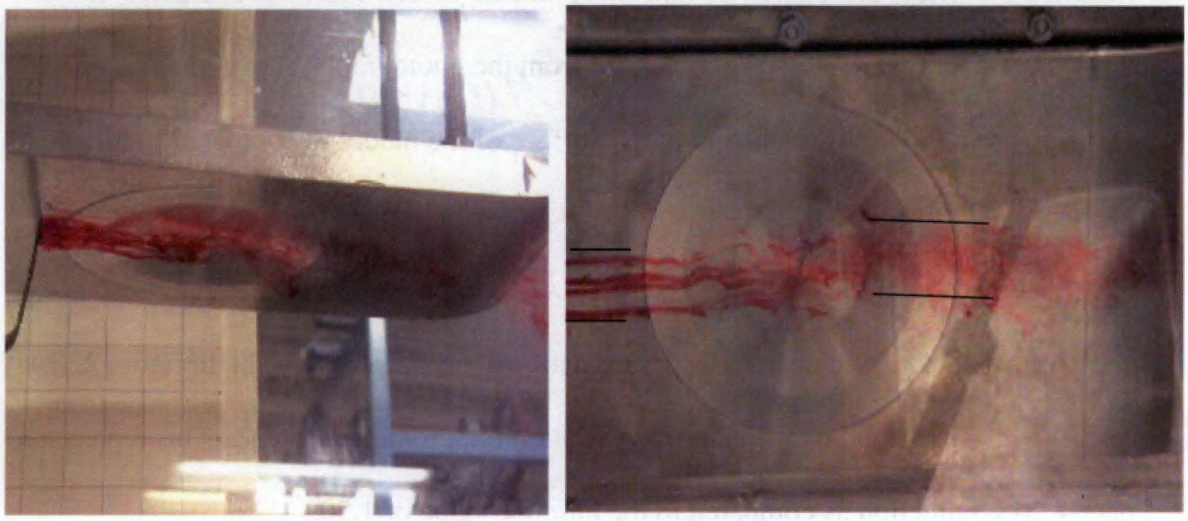
The area in yellow again represents low speed flow were some separation is occurring. The region in red, representing high pressure is a result of the flow being largely separated or stagnated. The red zone corresponds to the region in figure 18 where CP2 and CP3 are higher than that of the baseline. It is within this region that the majority of the separation and vortex shedding is occurring, thus the higher CP values. As can be seen in figure 19, there is a change in the middle region of the cavity, circled, as compared to the baseline cavity. It is evident that the pressure gradients have increased somewhat, reflecting increased velocity gradients. The increased gradients present are indicative of a minimal increase in the vorticity of the flow within the cavity. It was visually observed that the vortices shed from this design were somewhat tighter and shed

with a minimally decreased period as compared to the baseline. This is a factor in the reduction of the wake produced behind this dimple design. While this represents a slight improvement over the baseline dimple note that the separation zone is still relatively large, and thus a large wake is expected based on this observation.

Note that the red region where separation has occurred is somewhat more concentrated than that of the baseline dimple, indicative of a more concentrated initial distribution among the vortices when initially shed. The effect is not as apparent with this design as in following ones, however there is some improvement. This allows the vortices to have a lesser dispersion as they leave the dimple, contributing again to a reduction in the size of the wake produced by this configuration.

The higher kinetic energy of the flow in the region where vortex shedding is occurring, the vortices shed with a higher energy and therefore increased strength. This increase strength coupled with the reduction in initial dispersion allows the vortices to disperse less quickly. More importantly however, the increase strength of the vortices allows them to draw more energy from the main flow and thus the turbulent boundary layer receives greater energy as a result. This improves the overall ability of the flow to remain attached to the surface, and the wake production behind a golf ball would be reduced as a result. It would seem that the claim made by the designer of this configuration in reference 19 would indeed seem valid as a reduction in aerodynamic drag production would be expected based on this.

Figure 22 shows the size of the wake both from the top view and from a side view. It can be seen from this figure that there is still a large amount of turbulence associated with the flow that is leaving the cavity. The turbulence is somewhat



(a) (b)

Figure 22: Improved flow attachment of the flat bottomed dimple.

diminished as compared to the baseline flow which is attributed to the increased kinetic energy of the flow in the cavity, and its impact on the vortex shedding occurring in the cavity. Comparing the size of the wake relative to the size of the dye stream being fed to the dimple, the ratio is 1.22. This represents a 30% improvement over the dimple containing the baseline value of 1.50.

The vortices being shed show less dispersion compared to those observed with the baseline dimple, while as figure 22(a) shows it is also apparent that the vortices remain slightly closer to the surface of the model. This is due to the increased kinetic energy of the cavity flow, and an increase in the velocity gradients present in the cavity. As a

result, the vortices are shed in a more concentrated pattern and do not disperse as quickly. Note that while it is difficult to see from the photographs above, there is an improvement in the flow attachment to the surface of the model as compared to the baseline.

The portion of the flow attached to the surface remains so for a greater distance, indicative of its increased energy. Measurements of the size of the wake in figure 22(b) relative to the size of the dye stream show a ratio of approximately 1.22. This represents a nearly 20% reduction as compared to the baseline value of 1.50.

While it is obvious that there is an improvement over the baseline, the turbulence associated with this configuration is significant. Note that the vortices in the wake are still a large distance from the surface of the dimple.

4-3 Dimple Containing a Small Insert

The next configuration tested is shown in figure 23 with detailed drawings in Appendix A. In this design, an insert with a top diameter of 0.25 inches, reaching to 0.05 inches below the top level of the model surface and sloping at 45 degrees was employed. It was hypothesized that this would show an improvement in terms of the pressure distribution and the vortex shedding over the previous two designs.

The hoped improvement turned out to be the case. Figure 24 shows a snapshot of the circulation taking place inside the cavity. Figure 24 (a) shows the majority of the flow enters the cavity and turns inward as a result of flow attachment to the surface of the insert.

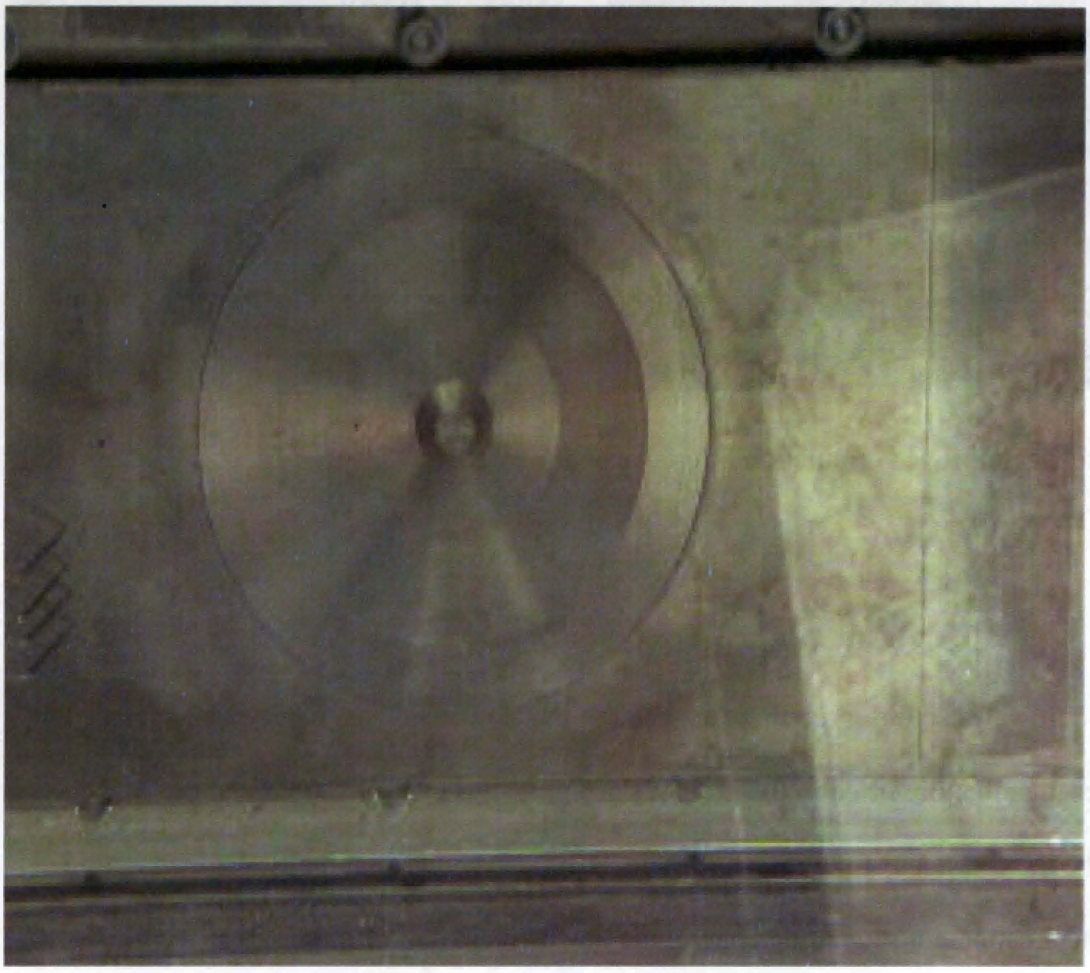
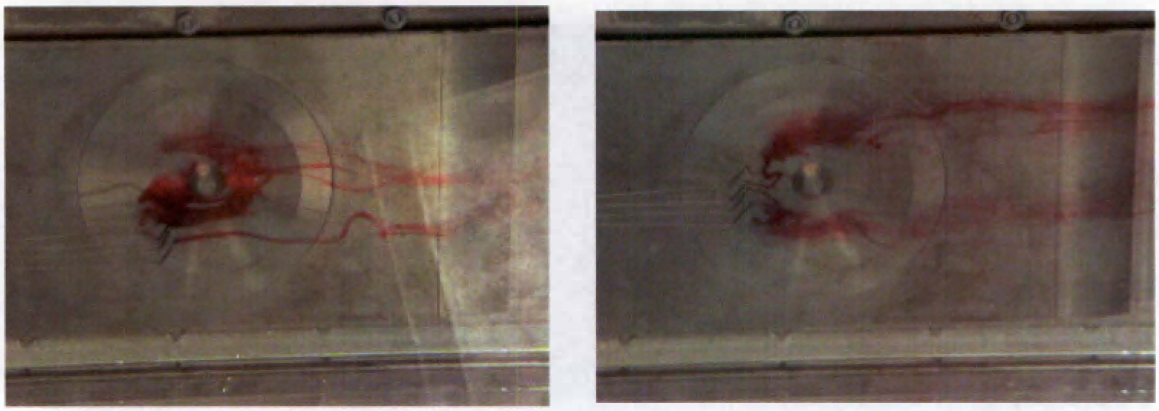


Figure 23: The dimple configuration containing a small insert



(a) (b)

Figure 24: Improved circulation of this design.

It was also observed that the speed of the flow inside the cavity was notably higher than that observed in the previous designs. It is clearly visible that the flow has attached to the sides of the insert. Figure 24(b) also shows that the flow is separating around an apparent stagnation zone in the downstream half of the insert in a cone surrounding the region 180 degrees from the leading edge of the cavity.

Figure 25 shows a plot of the pressure data collected for this configuration. Note that CP3 is not present. Data for this region was collected, however it was later omitted because the port for the pressure measurement was drilled through the top of the insert, and as a result, the data is not reflective of inside the cavity. In order to have a meaningful comparison of the performance of the various configurations, the plot in figure 25 was more appropriate.

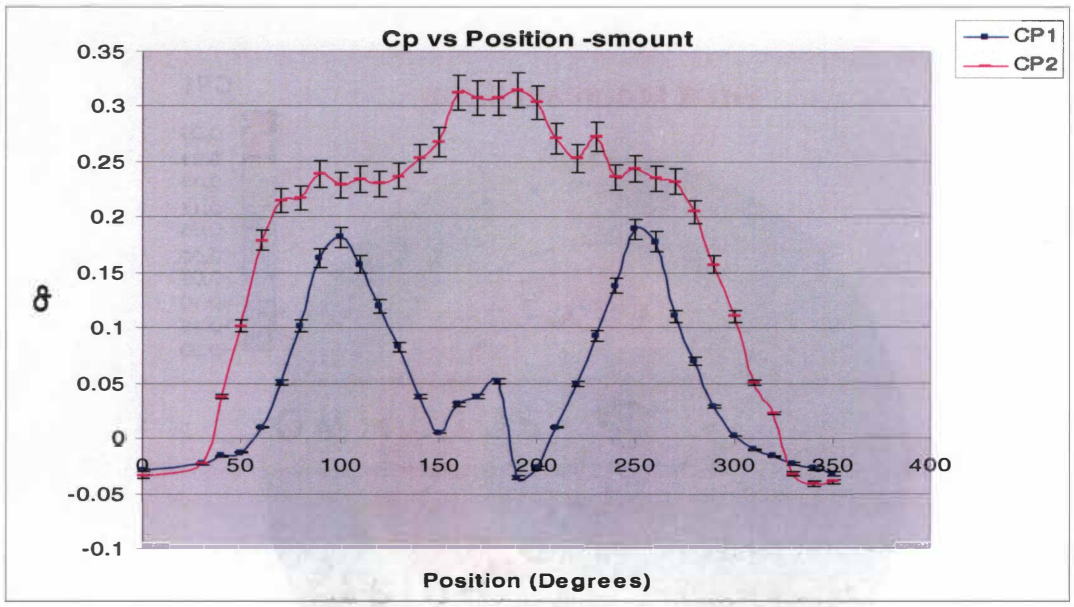


Figure 25: The pressure data collected for the dimple containing the small insert.

Interestingly, Cp1 for this configuration shows a very little change as compared to the previous configurations. There is however a small bump in CP1 from 150 degrees to 180 degrees, followed by a marked drop to 190 degrees.

The data collected for CP2 is very different in the region between 150 and 220 degrees. In this region a sharp increase in CP is obvious. The coefficient of pressure is approximately 40% higher than the baseline and approximately 15% higher than the flat bottomed dimple in this region.

The importance of this increase can be better viewed using the pressure contour plot obtained in figure 26. Note, however, that there is some uncertainty associated with this figure as the data is interpolated based on only the measurements obtained for 2 of the three pressure ports. The plot however does accurately reflect visual observations.

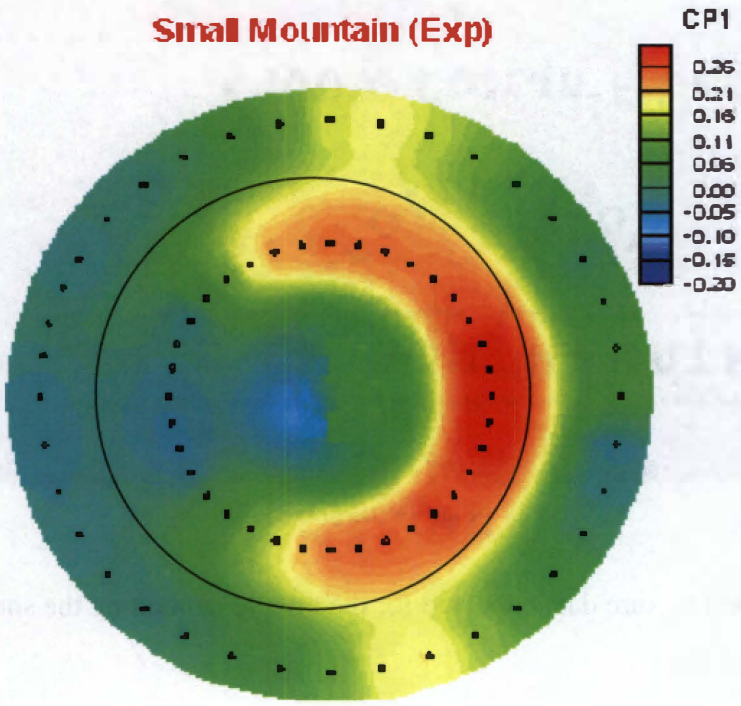


Figure 26: Pressure contour plot of dimple with small insert.

Physically, the area in red between 150-180 degrees corresponds to the region behind the insert where the evidence of the stagnation zone was viewed using dye. Note first of all that the red region, where the majority of vortex shedding is taking place is much more concentrated than that of both the baseline dimple and the configuration of section 3-2. This results in a decrease in the initial distribution pattern when the vortices are shed. There is still some shedding occurring in the region in orange, and this can be seen in the flow visualization runs. However, the majority of the vortex shedding is occurring in this red region. As with the design of section 4-2, a less dispersed pattern of vortices upon shedding is a contributing factor to the reduction in wake size behind the dimple.

Looking at the area circled in the center portion of figure 26, it is clearly evident that there is an increase in the velocity gradients. The gradients in the X-Y plane are greatly increased as can be seen by the changing in color from green to yellow and red, representing decreasing velocity as the stagnation point is approached. The area in green represents higher velocity circulation than was seen within the same region in the designs of the previous sections. Not evident in this plot is that there is also an increase in the gradient in the Z-direction. Attaching the flow to the surface of the insert also has the effect of bringing the cavity flow closer to the main flow. While the velocities in some regions are higher than the previous designs, the cavity flow here is much closer to the main flow, thus the gradients in this direction are greatly increased.

The reason for the increased gradients is the insert. As the flow is drawn into the cavity forward of the insert it is forced to attach to the insert. The flow must then increase in speed as it travels around the surface of the insert in order to maintain momentum [6]. The flow eventually separates in the region denoted in red in figure 26 shedding a higher energy vortex in the region of the rear stagnation point of the insert. The increase velocity due to flow attachment increases the velocity gradients in the vicinity of the center of the cavity.

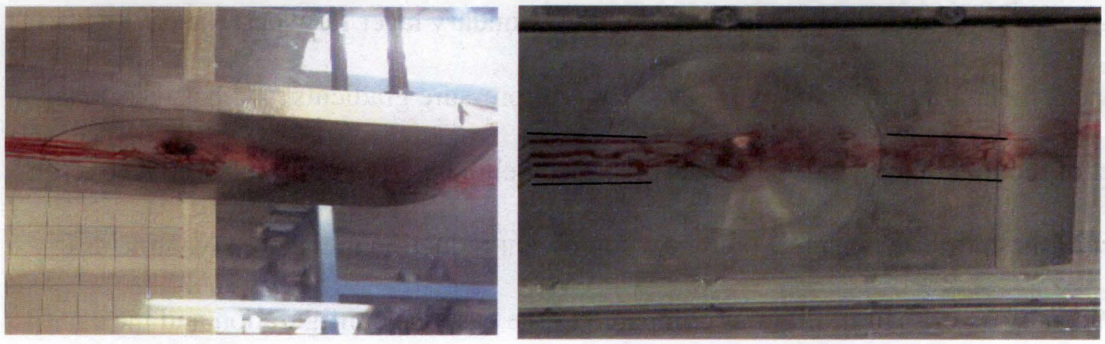
The increased velocity gradients concentrate the vorticity of this region of the flow as per equation (1). From the video taken during the flow visualization, there is a definite increase in the rate of vorticity production inside the cavity, indicative of the increase in vorticity.

It should be noted at this point that the total amount of energy present in the cavity does differ compared to that of the previous two designs. The cavity draws fluid

in from the main flow, which contains a given amount of energy, and the conservation of energy law still applies. In the previous designs, this energy is dispersed over the entire region of the dimple cavity, and thus the local velocities produced are low and the gradients are low because the energy concentration is low. The effect of the insert is to force the flow into a smaller area by having it attach to the insert. This concentrates the available energy into a smaller region and thus locally increases the velocities and gradients due to the increased energy concentration. Increasing the local kinetic energy is the mechanism responsible for the results of his discussion.

Observations of the vortices shed from this design show that the individual vortices are also smaller in size owing to the increased energy with which they are shed. This is apparent from figure 27(b) which also shows that the vortices shed are much less dispersed after they have left the cavity than the previous design. This is caused by the increased energy with which the vortices are shed from the region in red of figure 26. The decrease in dispersion results in a significantly reduced wake produced behind this design compared to the previous designs as the flow interacts with it.

The decreased dispersion, and smaller size of the vortices shed are a result of their improved energy concentration. Besides dispersing at a slower rate, the increased energy of these vortices improves their strength. The improved strength improves their ability to draw energy from the main flow resulting in a greater energy transport to the turbulent boundary layer. This effect was readily apparent in the flow visualization. Figure 27(a) shows both the reduced dispersion of the vortices traveling along the surface of the



(a) (b)

Figure 27: The increase size and turbulence of the wake created by this design is apparent when compared to those of the previous configurations.

model. It also shows a significant portion of the main flow remains attached to the surface of the model until the trailing edge of the model is reached. This is a clear indicator of the increased energy imparted to the boundary layer by the high energy vortices interacting with the main flow. This has the effect of reducing size of the turbulent wake.

Figure 27 (b) also shows that the wake has diminished in size substantially from the baseline and the flat bottomed dimple. Relative to the size of the dye stream, the wake size ratio is approximately 1. This represents a 20% improvement over the dimple containing the flat bottomed design and a 30% improvement over the baseline.

It is clear that this design represents a significant improvement over the baseline design and even the flat bottom design.

The reduced initial distribution area of the vortices when shed, combined with their apparent increased frequency, higher strength and reduced dispersion are all contributing factors in the observed reduction in the size of the wake generated by this dimple design.

The increased energy imparted to the boundary layer flow past the cavity also enhances the main flow's ability to resist adverse pressure gradients, and has the global effect of reducing the size of the wake generated behind a golf ball in flight. The overall effect of these improvements would be a significant reduction in the aerodynamic drag produced by a golf ball in flight as compared to the baseline configuration and the configuration of section 4-2.

4-4 Large Insert Dimple Design

In order to try and improve upon the performance of the dimple with the small insert, it was decided that a dimple with a larger insert should be studied. It was hypothesized that while there is significantly more recirculation in the small insert dimple as compared to the previous configurations, a larger insert would provide a greater surface still for flow to attach itself to. An even smaller insert in the cavity was considered, however because this would provide less surface area for the flow to attach to it was decided that an even smaller insert was not a design worth further consideration and testing.

The next question addressed was how much bigger the new insert should be. Too large, and there would not be enough of the bottom of the cavity exposed for recirculation to occur. Too small and there would not be a significant difference in the surface area presented by the insert and therefore very little difference in performance. It was therefore decided after some consideration that an insert with a top diameter of one inch would be appropriate. This led to the model shown in figure 28. While the base of this

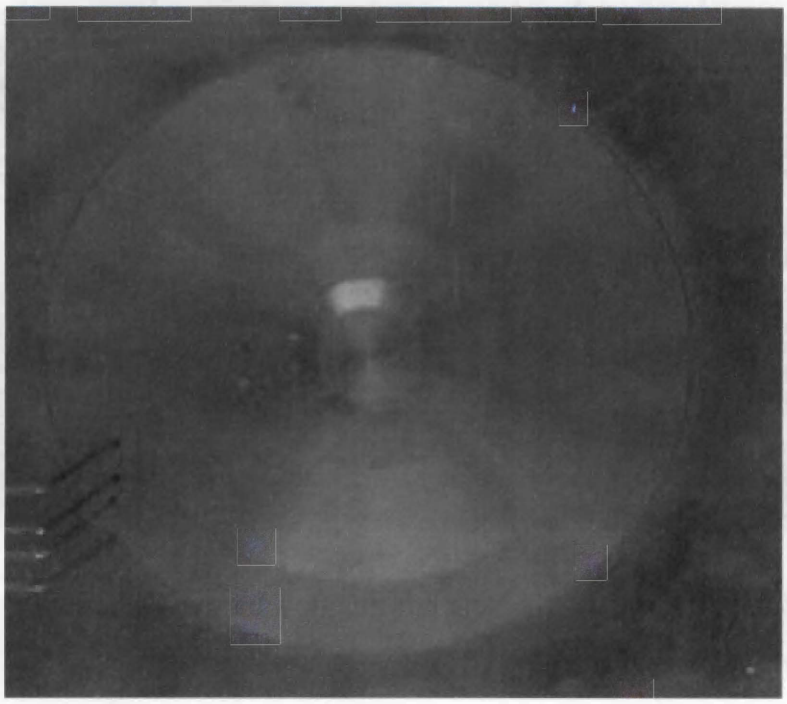
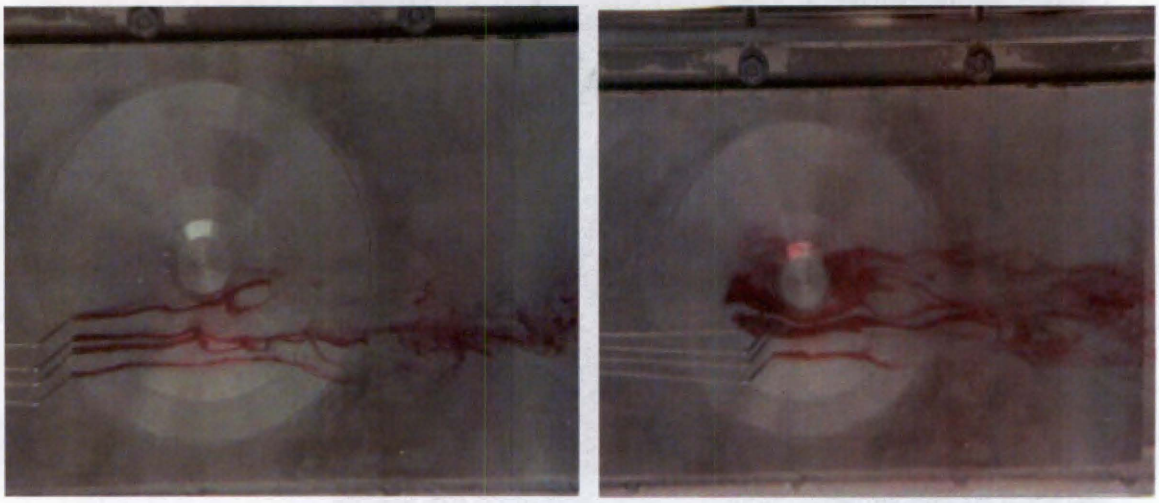


Figure 28: Dimple with large cavity insert.

insert is much larger than that of the previous model, there is still a substantial portion of the bottom of the cavity exposed and therefore available for recirculation.

Figure 29 shows the improvement in recirculation. In figure 29 (a), the dye has been introduced into the cavity from upstream, off center of the insert. It can be seen in the diagram that the flow has turned inward toward the flow attached to the insert. The circulation is even more evident in figure 29(b). This photograph was taken with the dye rake placed inside the cavity, off center. The dye in figure 29(b) can be seen surrounding the insert. It was visually observed that this happens quickly due to the speed with which the circulating flow is moving.



(a) (b)

Figure 29: Recirculation around the large insert. Note how the flow has turned around the base of the dimple.

There is also a leading edge stagnation point that is evident in figure 30. In this photo, the dye stream has been turned off for some time, and as can be seen the flow has moved almost entirely to the front area.

The most significant difference between figure 30 and figure 24 lies in CP2. In the regions between 50-140 degrees and 230-300 degrees there is a drop in CP2 on the order of 15-19%. This is indicative of faster flow velocity in this region.

When collecting the pressure measurements for this configuration, CP3 was again not included as the port was drilled through the top of the insert. Again, this was decided to be more representative of the flow as the pressure port for CP3 was drilled into the top of the large insert.

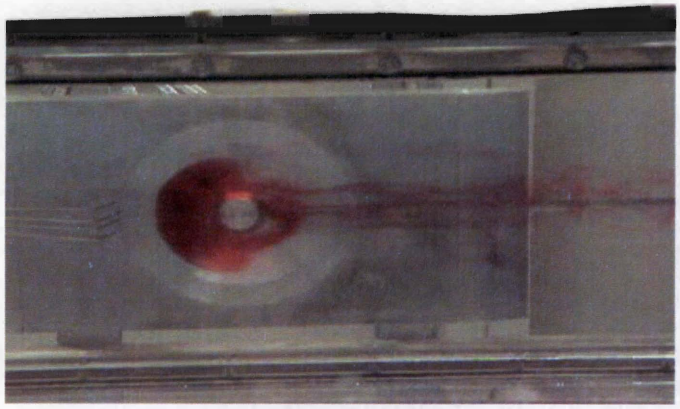


Figure 30: Evidence of the forward stagnation point.

Figure 31 is the plot obtained. Comparing it to the plot obtained for the dimple containing the small insert, there are some observations to note. The first concerns the plot for CP1.

It shows the same trend as all of the previous designs, including the small hump in the area of 150 degrees that was observed for the cavity containing the small insert. The difference here is that the hump is not as pronounced. The reason the hump exits in both this case and the small insert design is likely due to vortex shedding occurring on the surface of the insert in this region and thus the increase in pressure.

This is the area where the flow is attached to the side of the larger insert in this configuration, and thus supports the visual observations that the flow in this region is somewhat faster. The other difference between figures 30 and 24 is in the Peak CP values. In figure 31, it can be seen that the peak CP value occurs at approximately 180 degrees and has a value of approximately 0.32. This is an increase of nearly 10% over the peak value in the dimple with the previous design. This is also in a very concentrated area.

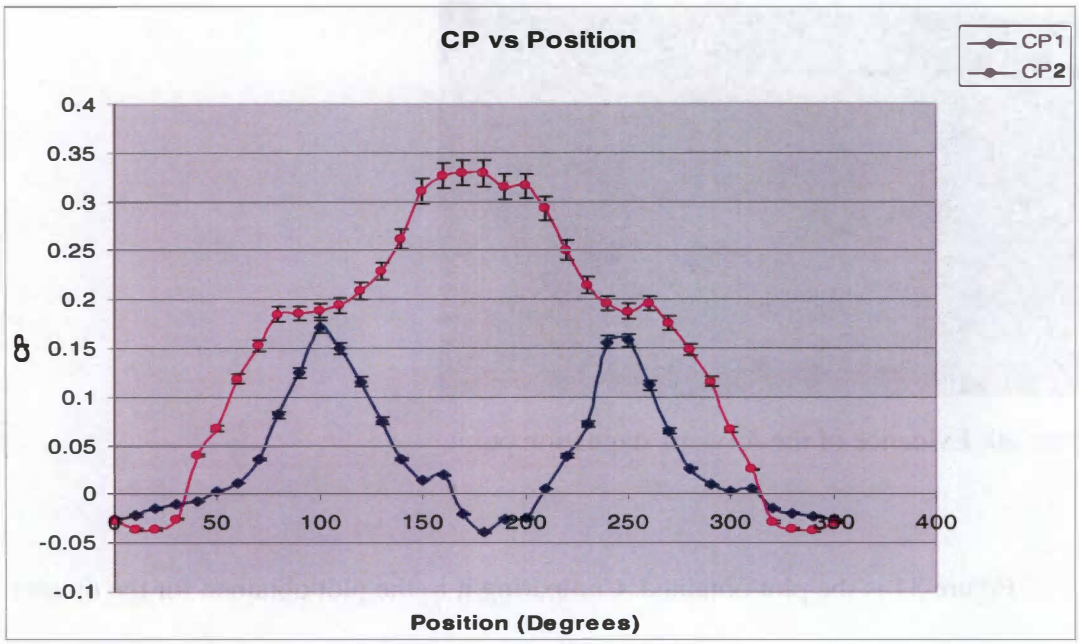


Figure 31: Pressure data obtained for the dimple containing a large insert.

The data in figure 31 was used to plot figure 32. Again a pressure coefficient contour flood plot was obtained by interpolating the data used to produce figure 31 and so it is subject to the same uncertainties as the other contour plots previously discussed. The significant differences with this design can be seen in the area circled in the middle of the contour plot of figure 32.

The green region represents lower pressures, and therefore much higher velocities, comparable with the configuration of section 3-3 and much improved over the designs of sections 4-1 and 4-2.

The same information can be gleaned from this plot as was obtained from the previous designs. The first observation deals with the region in red towards the rear enter

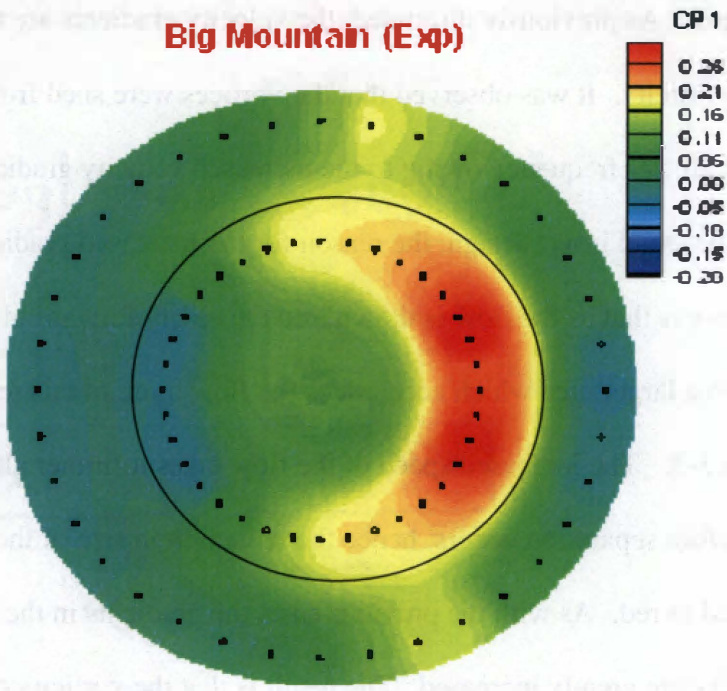


Figure 32: Pressure contour plot of the dimple containing the large insert.

of figure 32. Notice how this region is much smaller in area than the design of section 4-3. As discussed in previous sections, this is the region where the majority of the vortex shedding is taking place.

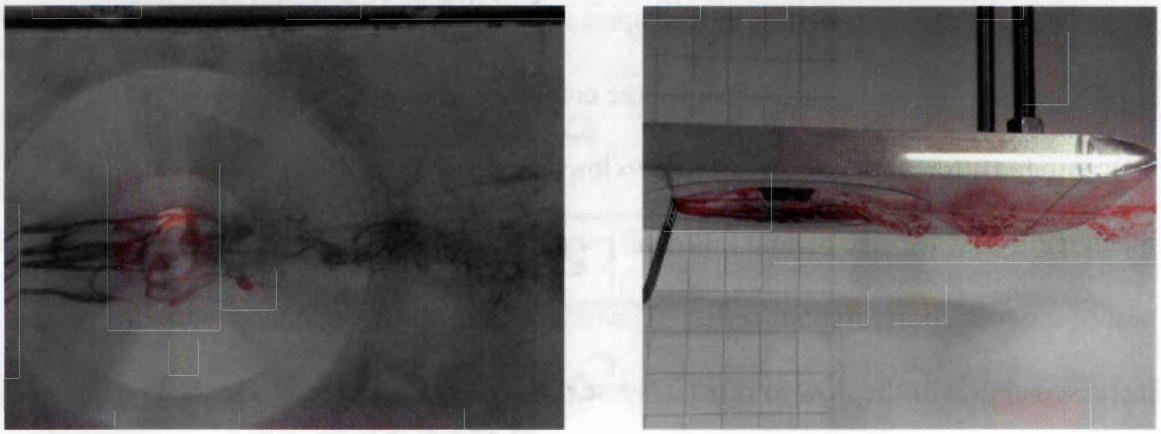
This region being small in size means that as with the previous design, the initial distribution pattern is more concentrated. In this case, this region is significantly reduced in size as compared to the small insert design. As with the previous design, this is a contributing factor in the reduction in the size of the wake produced behind this dimple design.

It is also evident from figure 32 that the velocity gradients between the red area and the green area within the circled region are very high as compared to all of the

previous designs. As previously discussed, the velocity gradients are responsible for determining the vorticity. It was observed that the vortices were shed from this cavity design at a much greater frequency owing to the increased velocity gradients.

As with the small insert design, the reason for the increased gradients is the insert. The difference here is that as the flow is drawn into the cavity forward of the insert it is forced to attach to a larger area which accelerates the flow more in this region than in the design of section 3-3. The increased speed of the flow takes it further along the circumference before separation occurs, hence the reduction in size of the shedding region represented in red. As with the previous case, the gradients in the vicinity of the center of the cavity are greatly increased. The result is that the vorticity of the flow inside the cavity is again increased causing the increase in the frequency of the shedding. Again, this is a factor in reducing the size of the wake shed from this design.

Because of the increased velocity, the vortices shed are again improved over the previous design in terms of their concentrated size. In figure 33 (a) it can be seen that the size of the vortices shed is very small as compared to the previous designs. This is owing to the increase in kinetic energy of the cavity flow. Additionally, the vortices do not disperse very quickly as can be seen in figure 33(b). The vortices remain very close to the surface of the model after leaving the cavity showing their ability to remain compact, unlike the previous designs which dispersed more quickly. Again, this is a substantial improvement over the previous designs and further reduces the size of the wake.



(a) (b)

Figure 33: The reduced wake and concentrated vortices shed from this design are much improved over the previous designs.

The increased kinetic energy also has the same effect as before in that the strength of the vortices shed are much stronger. This enhances their ability to draw energy from the main flow and pass it on to the boundary layer of the flow past the cavity. Again, looking at figure 33(b) we see the result. There is a significant portion of the flow that remains attached to the surface of the model until the end of the surface is reached. Again, this is beneficial as it means that the flow has a greater ability to resist adverse pressure gradients.

The combined effects of the higher energy cavity flow leads one to conclude that there would be a reduction in the size of the wake as compared to the previous designs. Comparing the size of the wake relative to the size of the dye stream being fed to the dimple, the ratio is 0.60. This represents a 40% improvement over the dimple containing the small insert, and a 50% decrease as compared to the flat configuration, and a 60% improvement over the baseline. It can also be seen that the dye stream is influenced by

the large insert as it is getting spread apart as the flow is forced to travel along its surface. As with the previous designs, the combined effects of the high energy, concentrated strong vortices better able to impart energy to the main flow results in a much reduced wake size behind this configuration. Additionally, this configuration is the best of the four configurations tested. The reduction in wake, combined with the increased ability of the flow to resist adverse pressure gradients results in the conclusion that the aerodynamic drag produced behind a ball employing this configuration would be significant as compared to the other three designs.

4-4-1 CFD Results

Figure 34 is a comparison of the results obtained experimentally on the left to that obtained through the use of CFD. The two contour plots of the pressure distribution are very similar. There is a difference in that the CFD code shows a forward stagnation region that is not present in the experimental data.

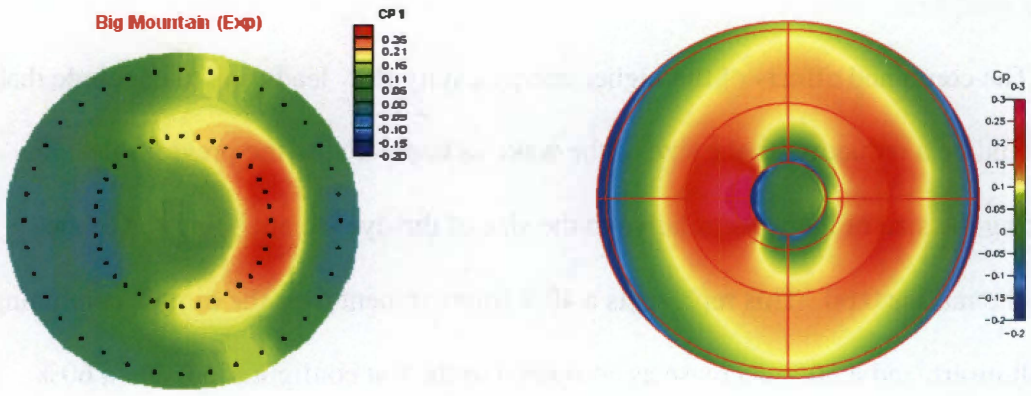
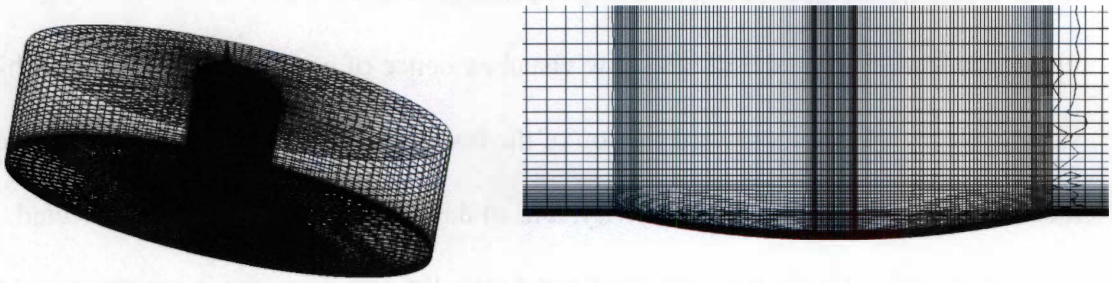


Figure 34: The experimental Cp distribution compared to CFD results.

It is expected that there would be a stagnation region in the forward portion of the insert and figures 30 and 33 both show visual evidence of it. It was observed that this stagnation region occurs toward the top of the insert, whereas the pressure ports were measuring data on the surface of cavity, and so data in this region was not collected. Again, this stagnation region was confirmed visually, and therefore is not presumed to be a discrepancy in the model.

The size of the region in red, where vortex shedding occurs, is nearly the same size in both plots. The CFD code also predicts slightly slower velocities around the outer edges of the dimple as the yellow region of the plot is somewhat larger than that shown in the experimental plot. This was the same trend that was noted in the baseline comparison. Note that the difference in the velocity is only minimally. As before, it is assumed that this difference is a result of the interpolation process that was used to plot the experimental results. It is therefore concluded that the CFD code CFD-ACE is able to successfully model physical processes and may be used in the future designs of dimples without necessarily undertaking physical experimentation.

Figure 35 (a) shows the overall grid for the big mountain case while figure 35 (b) is a slice of the cavity. Again, it extends to 5 times the dimple diameter in height and length.



(a) (b)

Figure 35: The grid used for the CFD simulation.

Chapter 5
Conclusions and Recommendations

5-1 Concussions

In this study, the reduction in the size of the wake, and therefore the drag produced, by a golf ball dimple was studied by means of increasing the strength of the vortices shed within the dimple cavity. Through the use of flow visualization and pressure distribution measurement, it was determined that an insert of sufficient size and height installed in the cavity provided a means of increasing the strength of the vortices shed by increasing the velocity gradients present within the cavity. The results were compared to the computational fluid dynamics results from a commercial code CFD-ACE in order to validate its use in future work. The following conclusions were obtained:

1. The wake behind a golf ball dimple may be significantly reduced in size through the strengthening of the vortices shed from within the dimple.

2. An effective way to increase the strength of the vortices shed is to have a large insert within the cavity that provides a surface for circulating flow to attach to. The resulting increase in velocity gradients provides the means through which the vortex strength is improved.

3. The Stronger vortices draw energy from the main flow and impart that energy to the boundary layer near the surface of the ball. This provides the boundary layer more energy enabling it to remain attached longer, resulting in a reduced wake.

4. CFD modeling reasonably simulates the cavity flow studied in this study. It may be used with confidence in future, with care, and may be used to provide details of the flow that can not be measured.

5-2 Recommendations

The following are recommendations for future work:

1. CFD may be used to explore dimple inserts of various sizes in order to determine the effect of minimal changes.
2. More sophisticated testing is required to obtain a quantitative estimate of the reduction in C_D produced by the reduction in wake size. And determine the interaction between successive dimples of the new design developed here in order to determine an optimum distribution.
3. Test a scaled or full size golf ball to validate the results obtained in this work.

References

References

1. http://observe.arc.nasa.gov/nasa/Tech_Twice/Tech_twice2.html
2. Kimura T and Tsutahara M, "Fluid Dynamic Effects of Grooves on Circular Cylinder Surface", AIAA Journal, Vol.29, December 1991.
3. L.L Ting, "Effects of Dimple Size and Depth on Golf Ball Aerodynamic Performance", FEDSM2003-45081, Proceedings of FEDSM'03 4th ASME_JSME Joint Fluids Engineering Conference Honolulu, Hawaii, July 6-10, 2003.
4. L.L Ting, "Application of CFD Technology analyzing the Three Dimensional Aerodynamic Behavior of Dimpled Golf Balls", IMEC2002-32349, Proceedings of IMECE2002 ASME International Mechanical Engineering Congress & Exposition, November 17-22, 2002, New Orleans, Louisiana.
5. Bearman, P.W., and Harvey, J.K., "Golf Ball Aerodynamics," Aeronautical Quarterly, May 1976, pp. 112-122.
6. White F.M, "Viscous Fluid Flow", 2nd ed. McGraw-Hill, USA, 1991.
7. "Golf Balls, Slicing Through the Hype" Consumer Report Magazine, pp. 30-33, May 2006
8. Rabinovich, S., "Measurement Errors: Theory and Practice", American Institute of Physics, New York, 1995.
9. Saffman, P.G., "Vortex Dynamics", Cambridge University Press, 1997
10. Batchelor, G.K., "An introduction to Fluid Dynamics", Cambridge University Press, New York, 1992.
11. Lugt, Hans, J., "An Introduction to Vortex Theory", Vortex Flow Press, Inc., 1996.

12. Stephens, L.J., " Theory and Problems of Statistics", 3rd Ed., Schaum's Outline Series, McGraw-Hill, Chicago, 1999.

13. WU, J.C, "Elements of Vorticity Dynamics", Tsinguhua University, Springer, 2006.

14. McDaniels, M.D., "Background and Theoretical Considerations For Utilizing Water Tunnel Flow Visualization", Master's Dissertation, UTSI, 1996.

15. Aoyama Et al., United States Patent No. US 6,969,327, 29 Nov, 2005.

16. Ogg et al., United States Patent No. 6,979,272, 27 Dec, 2005.

17. United States Patent No. 6,979,271, 27 Dec., 2005.

18. Wilson Co, United States Patent No. 6,979,567, 10 Dec, 1996

19. Raymer, D.P., "Aircraft Design, an Experimental Approach", 3rd Ed., AIAA, Virginia, 1999.

20. Karamcheti, K., "Principles of Ideal-Fluid Aerodynamics", Krieger Publishing Company, Florida, 1980.

21. Vakili, A.D., University of Tennessee Space Institute, 2005-2006.

22. CFD-ACE Command Language Manual, Version 6.0, Feb. 2005.

23. Vector Launch Monitor, Operator's Manual, July, 2005

24. Golf Digest Magazine, July 2005.

25. Van Dyke, M. "An Album of Fluid Motion" Parabolic Press, California

Appendix A

Drawings

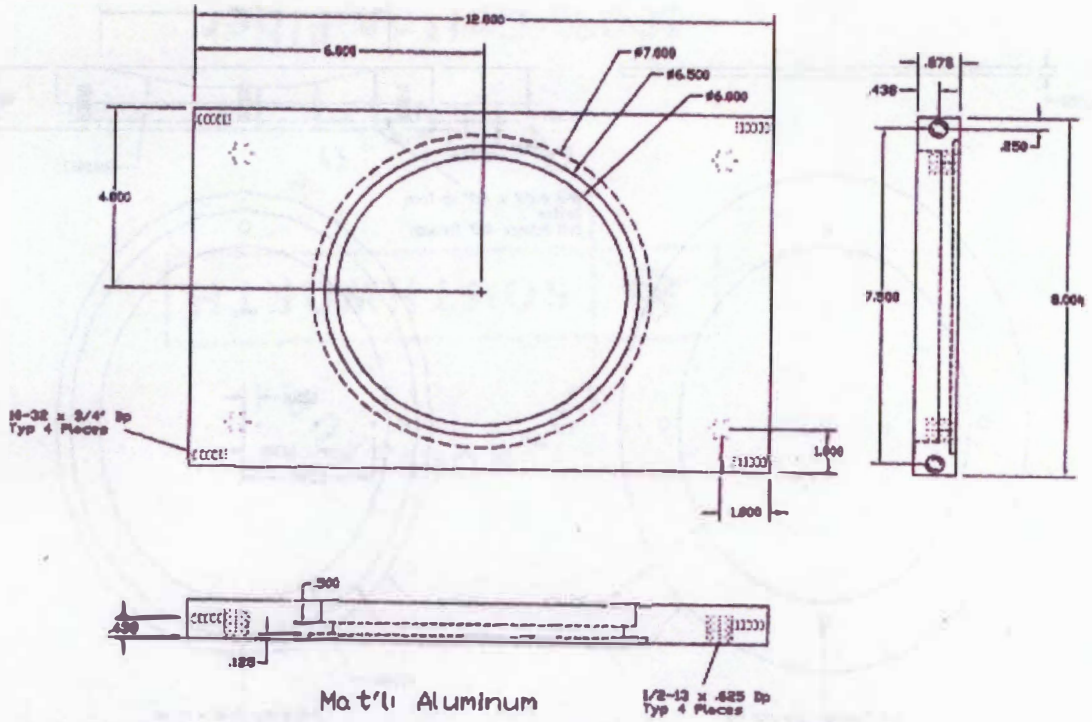


Figure A-1: The middle of the support Structure.

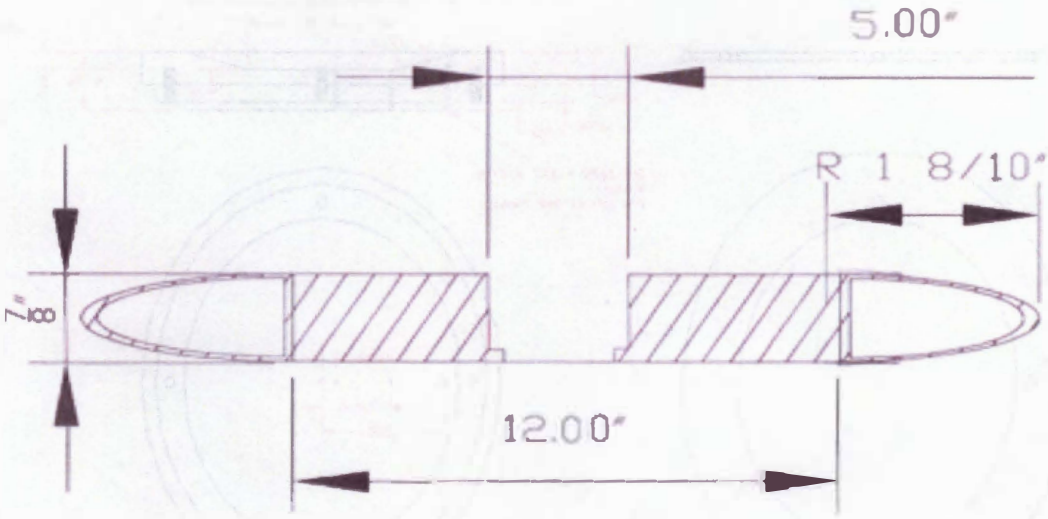


Figure A-2: The main support structure

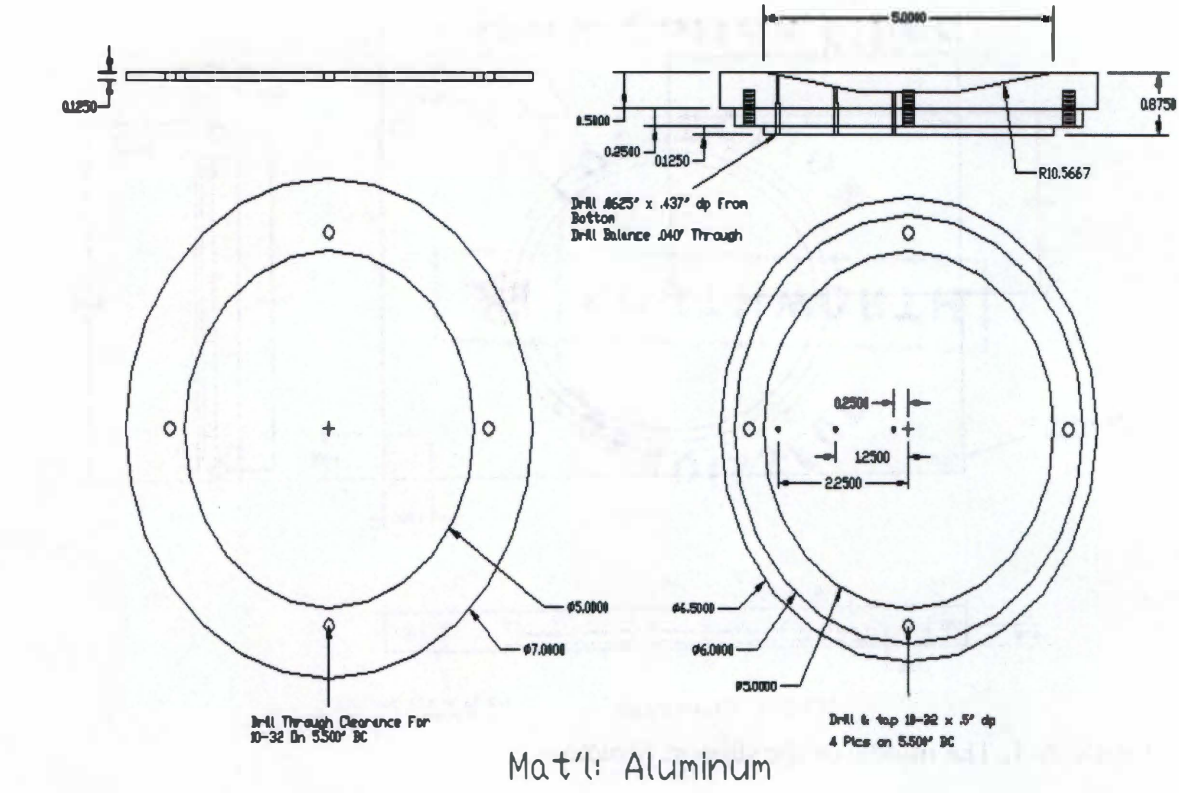


Figure A-3: The baseline Dimple

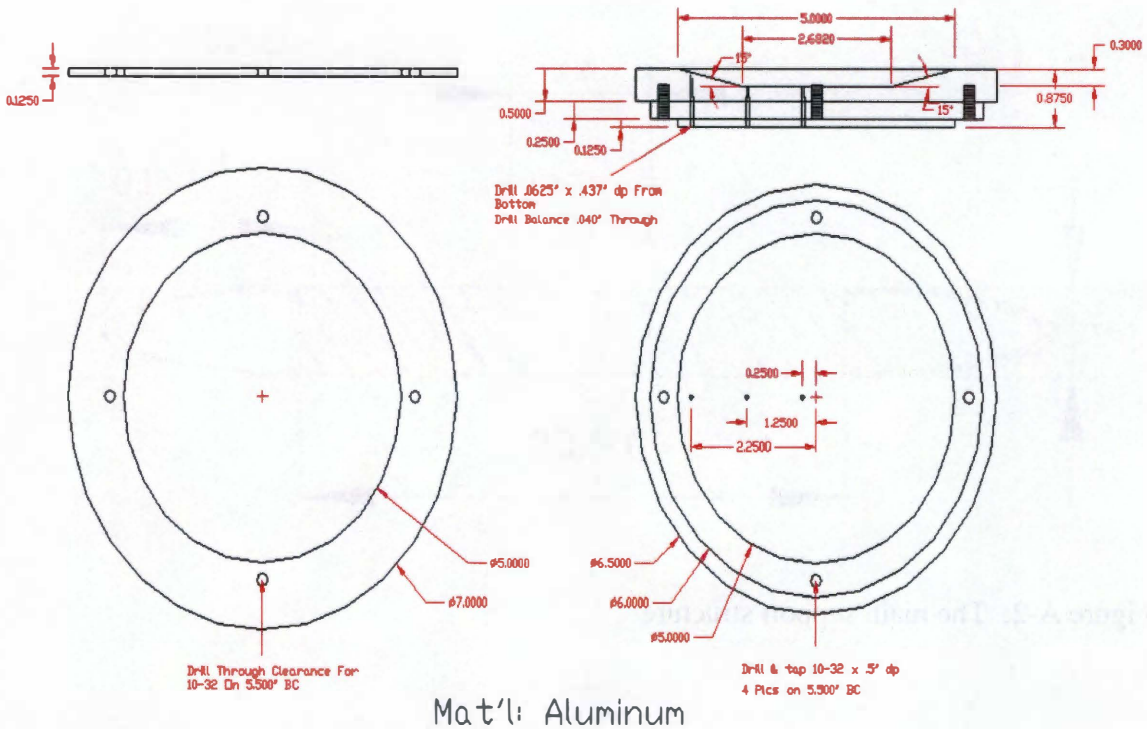


Figure A-4: The flat Bottomed Dimple

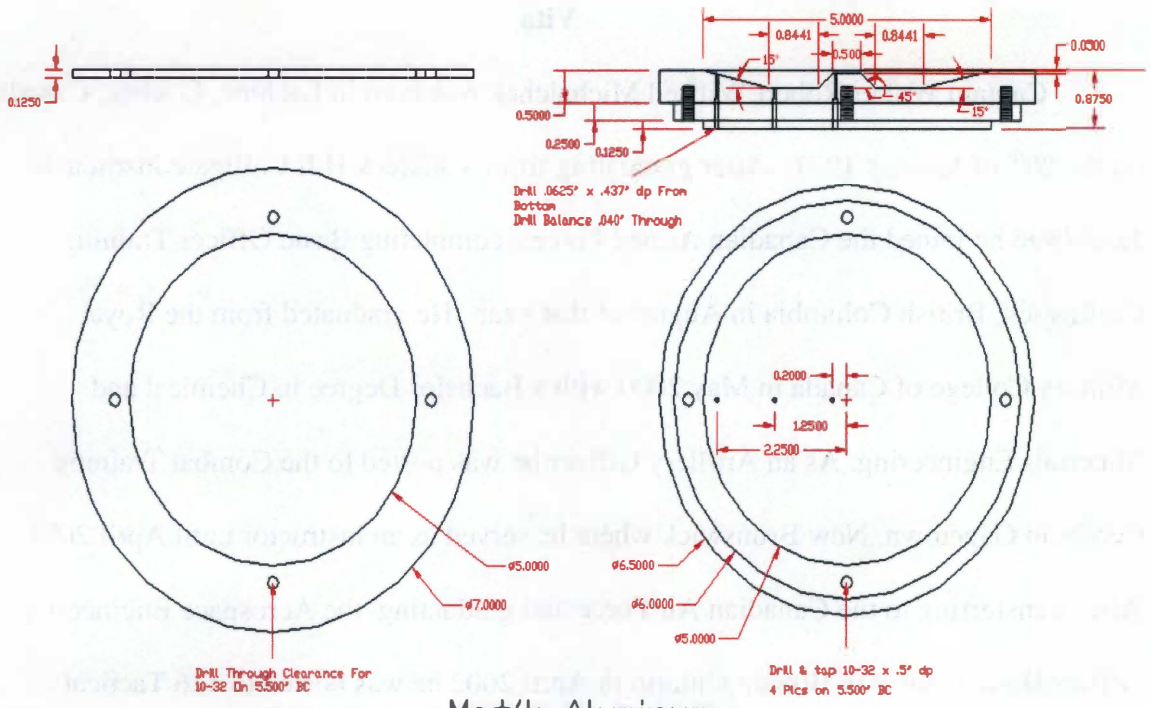


Figure A-5: The Small Insert Dimple

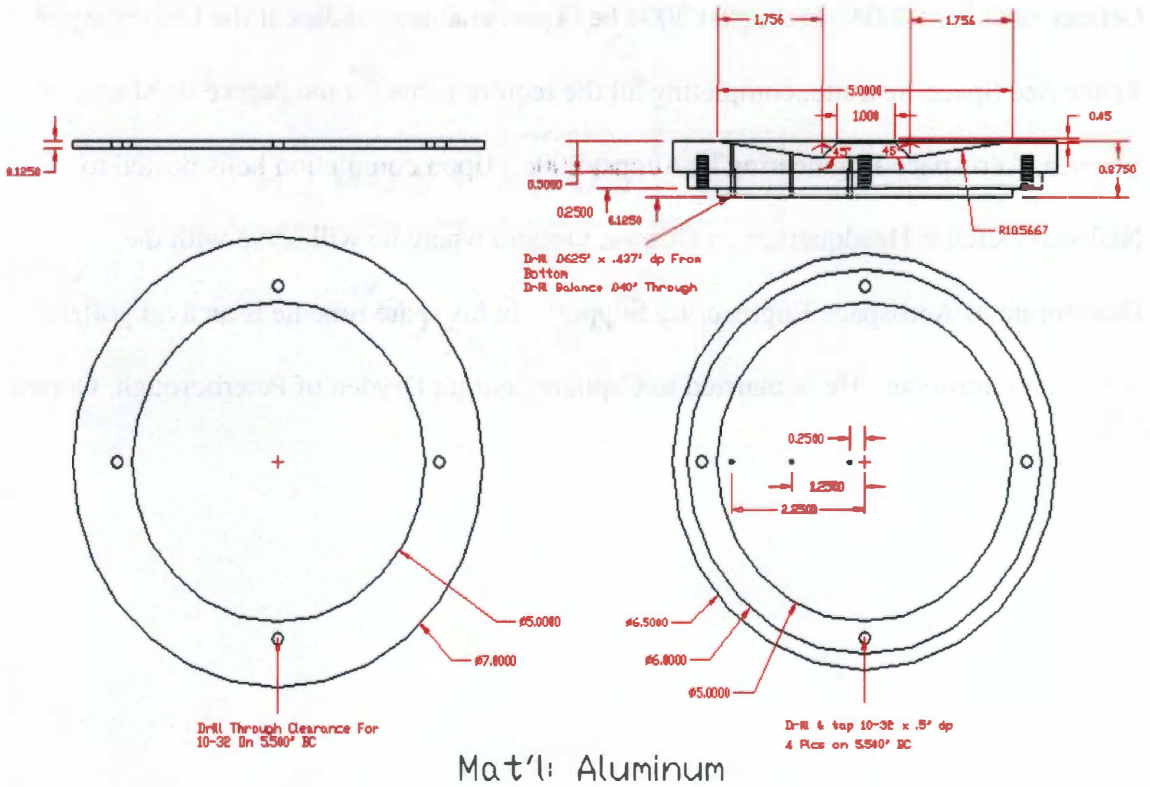


Figure A-6: The Large Insert Dimple

Vita

Captain Walter Robert Wilfred Michalchuk was born in Lachine, Quebec, Canada on the 20th of January 1977. After graduating from Vankleek Hill Colligate Institute in June 1996 he joined the Canadian Armed Forces, completing Basic Officer Training in Chilliwack, British Columbia in August of that year. He graduated from the Royal Military College of Canada in May 2000 with a Bachelor Degree in Chemical and Materials Engineering. As an Artillery Officer he was posted to the Combat Training Center in Gagetown, New Brunswick where he served as an instructor until April 2001. After transferring to the Canadian Air Force and graduating the Aerospace Engineering Officer Basic Course in Borden Ontario in April 2002 he was posted to 416 Tactical Fighter Squadron in Cold Lake, Alberta where he served as the Aircraft Production Officer until July 2004. In August 2004 he began graduate studies at the University of Tennessee Space Institute, completing all the requirements for the degree of Master of Science, Aerospace Engineering in August 2006. Upon completion he is posted to National Defense Headquarters in Ottawa, Ontario where he will serve with the Directorate of Aerospace Engineering Support. In his spare time he is an avid golfer, archer and musician. He is married to Captain Georgia Dryden of Peterborough, Ontario.

5873 8921 18
84/04/07 UM 凱利Group